AGU PUBLICATIONS

JGR

Journal of Geophysical Research: Atmospheres

RESEARCH ARTICLE
10.1002/2014JD021770

Key Points:
- Ice core 17O-xs changes in West Antarctica are comparable to East Antarctica
- Antarctic snow formation under supersaturated conditions results in lower 17O-xs
- Sea ice changes, and lower temperature, explain glacial-Holocene 17O-xs changes

Supporting Information:
- Readme
- Figure S1
- Figure S2
- Figure S3
- Figure S4
- Figure S5
- Data S1
- Table S1
- Text S1

Correspondence to:
S. W. Schoenemann,
schoes@uw.edu

Citation:
Schoenemann, S. W., E. J. Steig, Q. Ding, B. R. Markle, and A. J. Schauer (2014), Triple water-isotopologue record from WAIS Divide, Antarctica: Controls on glacial-interglacial changes in $^{17}O_{excess}$ of precipitation, *J. Geophys. Res. Atmos.*, *119*, 8741–8763, doi:10.1002/2014JD021770.

Received 14 MAR 2014
Accepted 13 JUN 2014
Accepted article online 18 JUN 2014
Published online 28 JUL 2014

Triple water-isotopologue record from WAIS Divide, Antarctica: Controls on glacial-interglacial changes in $^{17}O_{excess}$ of precipitation

Spruce W. Schoenemann[1], Eric J. Steig[1], Qinghua Ding[1], Bradley R. Markle[1], and Andrew J. Schauer[1]

[1]IsoLab, Department of Earth and Space Sciences, University of Washington, Seattle, USA

Abstract Measurements of the $^{17}O_{excess}$ of H_2O were obtained from ice cores in West and East Antarctica. Combined with previously published results from East Antarctica, the new data provide the most complete spatial and temporal view of Antarctic $^{17}O_{excess}$ to date. There is a steep spatial gradient of $^{17}O_{excess}$ in present-day precipitation across Antarctica, with higher values in marine-influenced regions and lower values in the East Antarctic interior. There is also a spatial pattern to the change in $^{17}O_{excess}$ between the Last Glacial Maximum (LGM) and Holocene periods. At coastal locations, there is no significant change in $^{17}O_{excess}$. At both the West Antarctic Ice Sheet Divide site and at Vostok, East Antarctica, the LGM to Early Holocene change in $^{17}O_{excess}$ is about 20 per meg. Atmospheric general circulation model (GCM) experiments show that both the observed spatial gradient of $^{17}O_{excess}$ in modern precipitation, and the spatial pattern of LGM to Early Holocene change, can be explained by kinetic isotope effects during snow formation under supersaturated conditions, requiring a high sensitivity of supersaturation to temperature. The results suggest that fractionation during snow formation is the primary control on $^{17}O_{excess}$ in Antarctic precipitation. Variations in moisture source relative humidity play a negligible role in determining the glacial-interglacial $^{17}O_{excess}$ changes observed in Antarctic ice cores. Additional GCM experiments show that sea ice expansion increases the area over which supersaturating conditions occur, amplifying the effect of colder temperatures. Temperature and sea ice changes alone are sufficient to explain the observed $^{17}O_{excess}$ glacial-interglacial changes across Antarctica.

1. Introduction

Measurements of the stable isotope ratios of water (δD and δ^{18}O) in polar precipitation have long been used in ice core studies [*Dansgaard*, 1964; *Merlivat and Jouzel*, 1979; *Gat*, 1996; *Jouzel et al.*, 2003]. A recent innovation is the development of methods for obtaining precise measurements of the third water isotope ratio, δ^{17}O [*Baker et al.*, 2002; *Barkan and Luz*, 2005], complementing traditional measurements of δD and δ^{18}O. Combined measurements of δ^{18}O and δ^{17}O can be expressed with the parameter $^{17}O_{excess}$:

$$^{17}O_{excess} = \ln\left(\delta^{17}O + 1\right) - 0.528 \times \ln\left(\delta^{18}O + 1\right) \quad (1)$$

where δ^{18}O and δ^{17}O are unitless ratios defined by $\delta^{i}O = {}^{i}R_{sample}/{}^{i}R_{VSMOW} - 1$, and ${}^{i}R$ is the ratio of isotopologue $H_2{}^{i}O$ to the common isotopologue $H_2{}^{16}O$. Variations in $^{17}O_{excess}$ are generally several orders of magnitude smaller than variations in δ^{18}O and are conventionally expressed in per meg (10^{-6}) or ppm.

Like the better known deuterium excess, $d_{excess} = \delta D - 8 \times \delta^{18}O$, $^{17}O_{excess}$ is sensitive to kinetic fractionation. The d_{excess} in precipitation has frequently been interpreted as a proxy for moisture source conditions because it is sensitive to both temperature and humidity during evaporation. However, this interpretation is complicated by the fact that d_{excess} is not a conservative tracer in the atmosphere, even under purely equilibrium conditions [*Jouzel and Merlivat*, 1984; *Petit et al.*, 1991; *Kavanaugh and Cuffey*, 2003; *Masson-Delmotte et al.*, 2008; *Uemura et al.*, 2012]. The theoretical advantage of $^{17}O_{excess}$ is that it is insensitive to evaporation temperature [*Barkan and Luz*, 2007; *Risi et al.*, 2010a] and is less sensitive than d_{excess} to equilibrium fractionation processes during the formation of snow. In combination with δ^{18}O and d_{excess}, $^{17}O_{excess}$ offers a potential means to disentangle the competing effects of fractionation during evaporation, in transport, and during the formation and deposition of precipitation.

Both theory and experimental results show that an excess of ^{17}O in meteoric water originates from evaporation of ocean water into undersaturated air and is negatively correlated with relative humidity [*Barkan and Luz*, 2007;

Luz and Barkan, 2010; *Risi et al.*, 2010a]. Variations of $\delta^{17}O$ and $\delta^{18}O$ stem from the difference in saturation vapor pressures between the light and heavy isotopes, resulting in vapor liquid equilibrium fractionation expressed as $\theta = \ln(^{17}\alpha)/\ln(^{18}\alpha)$, where ($\theta_{eq} = 0.529$) and α is the fractionation factor [*Matsuhisa et al.*, 1978]. The greater diffusivity of light isotopes leads to kinetic fractionation, with $\theta_{diff} = 0.518$ [*Barkan and Luz*, 2007]. Theoretically, kinetic isotopic fractionation from diffusive transport of water vapor in air should dominate the mean $^{17}O_{excess}$ in water vapor at the ocean surface. As expected, elevated values of $^{17}O_{excess}$ are observed in marine vapor and in meteoric waters, including polar snow [*Gat*, 1996; *Barkan and Luz,* 2005, 2007; *Landais et al.*, 2008; *Uemura et al.*, 2010].

During snow formation in the polar regions, the condensation of water vapor to liquid or ice typically occurs above saturation (i.e., >100% relative humidity). In this environment, the vapor pressure surrounding a water droplet or ice crystal is greater than that of the saturated vapor pressure for the condensing surface, resulting in supersaturation. In Antarctica, the lack of ice nuclei onto which water vapor can condense results in highly supersaturated conditions. The strong gradient in vapor pressure between the supersaturated water vapor and the ice surface favors preferential removal of $H_2{}^{17}O$, leaving the remaining vapor enriched in $H_2{}^{18}O$ relative to the global meteoric water line (GMWL = 0.528). This kinetic fractionation process during ice crystal formation is due to the greater amount of molecular diffusion that occurs for the lighter isotopologue ($H_2{}^{17}O$). Note that relative to $H_2{}^{16}O$, both the heavy isotopologues ($H_2{}^{17}O$ and $H_2{}^{18}O$) are still preferentially removed through equilibrium fractionation and the vapor becomes more depleted in $\delta^{17}O$ and $\delta^{18}O$. Equilibrium fractionation alone would preferentially deplete $H_2{}^{18}O$ in the water vapor and therefore result in more positive $^{17}O_{excess}$ values. However, the competing influence of kinetic fractionation under stronger supersaturation conditions dominates the total effective fractionation. This results in progressively lower $^{17}O_{excess}$ as condensation proceeds (e.g., for snowfall forming from an air mass moving further into the Antarctic interior).

The normalized relative humidity (hereafter, rh_n) immediately above the ocean surface is the main factor controlling $^{17}O_{excess}$ in the marine boundary layer, though the degree of turbulence (i.e., the wind speed) affects the sensitivity [*Landais et al.*, 2008; *Risi et al.*, 2010a]. The rh_n is defined as the water vapor concentration in the free air divided by the saturated vapor concentration at the temperature of the ocean surface [*Gat*, 1996; *Barkan and Luz*, 2007; *Uemura et al.*, 2010; *Risi et al.*, 2010a]:

$$rh_n = rh_a \times \frac{q_{sat}(T_a)}{q_{sat}(T_s)} \tag{2}$$

Previous work suggested $^{17}O_{excess}$ to be only weakly influenced by fractionation during precipitation, and it was therefore expected that $^{17}O_{excess}$ in polar snow and ice could be used as a proxy for the humidity in the marine boundary layer over the moisture source areas where polar moisture originates [*Barkan and Luz,* 2005, 2007; *Landais et al.*, 2008; *Luz and Barkan*, 2010; *Risi et al.*, 2010a; *Winkler et al.*, 2012; *Landais et al.*, 2012a]. In particular, *Landais et al.* [2008] interpreted the 20 per meg $^{17}O_{excess}$ decrease between the Early Holocene (EH, 12–9 ka) and Last Glacial Maximum (25–20 ka) in the Vostok ice core to indicate a 20% rh_n increase over the average glacial ocean moisture source for East Antarctic precipitation. However, two additional $^{17}O_{excess}$ records from East Antarctica (European Project for Ice Coring in Antarctica (EPICA) Dome C and Talos Dome) show smaller degrees of Last Glacial Maximum (LGM) to EH change than at Vostok. *Winkler et al.* [2012] showed that this observation made the interpretation of $^{17}O_{excess}$ change at Vostok as a change in source region rh_n problematic. They proposed several mechanisms: different moisture source regions reflecting different rh_n and moisture trajectories and kinetic fractionation with a stronger supersaturation sensitivity to temperature, in order to explain the different $^{17}O_{excess}$ evolution between cores. It was suggested earlier by *Miller* [2008] that the relatively large magnitude of LGM to EH $^{17}O_{excess}$ change observed at Vostok may reflect the influence of stratospheric water vapor with a strong anomalous $^{17}O_{excess}$ signature. Interpretation of $^{17}O_{excess}$ in Antarctic ice cores thus remains ambiguous.

To date, all records of Antarctic $^{17}O_{excess}$ variability have come from East Antarctica. Here we contribute new $^{17}O_{excess}$ data from West Antarctica, including a ~25,000 year long record from an ice core at the central West Antarctic Ice Sheet divide (WAIS Divide). We also present new deuterium excess data from the WAIS Divide ice core. As recommended by *Uemura et al.* [2012] we adopt a natural log definition of

d_{excess} (hereafter, d_{ln}). *Uemura et al.* [2012] calculated a second-order polynomial best fit to the natural log of the isotopic data from the Global Network of Isotopes in Precipitation and a compilation of Antarctic isotope data [*Masson-Delmotte et al.*, 2008]:

$$d_{ln} = \ln(\delta D + 1) - \left(-2.85 \times 10^{-2} \left(\ln\left(\delta^{18}O + 1\right)\right)^2 + 8.47 \left(\ln\left(\delta^{18}O + 1\right)\right)\right) \quad (3)$$

The use of d_{ln} better accounts for differences in temperature sensitivity of equilibrium fractionation between δD and δ^{18}O than does the traditional d_{excess}. The use of d_{ln} also reduces the impact of glacial-interglacial changes in the isotopic concentration of seawater, which requires a significant correction for d_{excess} [*Stenni et al.*, 2010b].

Together, the new data provide a more complete picture of the spatial distribution of $^{17}O_{excess}$ across Antarctica, and allow us to better assess the controls on $^{17}O_{excess}$ on glacial-interglacial timescales.

2. Methods

The WAIS Divide ice core (WDC) was drilled over a 5 year period, reaching a depth of 3405 m in 2011. The core was drilled at latitude 79°28.06'S and longitude 112°05.2'W, about 24 km west of the Ross-Amundsen ice flow divide and 160 km east of the Byrd Station ice core site. The elevation at the ice core site is 1766 m; the modern accumulation rate is 22 cm a^{-1} (ice equivalent) and the mean annual temperature is approximately −30°C. The age of the oldest recovered ice is ~68 ka [*WAIS Divide Project Members*, 2013].

We measured $^{17}O_{excess}$ on the WDC using methods developed by *Baker et al.* [2002] and *Barkan and Luz* [2005, 2007] and described in detail in *Schoenemann et al.* [2013]. Briefly, water is fluorinated with CoF_3 to produce O_2 [*Barkan and Luz*, 2005], which is then carried by helium to a molecular sieve trap as in *Abe* [2008]. The O_2 sample is analyzed for *m/z* 32, 33, and 34 abundance ratios on a dual-inlet ThermoFinnigan MAT 253 isotope ratio mass spectrometer (ThermoElectron, Bremen, Germany) to determine δ^{18}O and δ^{17}O values with reference to O_2 gas.

Samples from the WDC were measured every 20 and 10 m for Holocene age and glacial age samples, respectively. The measurements cover from ~25 ka to the present, spanning depths 2600 m to 0 m in the WDC. We used both an internal water standard (WAIS Water) and the Vienna Standard Mean Ocean Water (VSMOW) 2, Standard Light Antarctic Precipitation (SLAP)/SLAP2, and GISP standards from the International Atomic Energy Agency, measured after every 10–15 samples to calibrate and verify the performance of both the fluorination line and the mass spectrometer. All samples were reproduced in duplicate or greater. The measured δ^{18}O and δ^{17}O data were corrected to the VSMOW-SLAP scale using the normalization technique of *Schoenemann et al.* [2013]. The reproducibility associated with each sample is given by the population standard deviation (6 per meg) of the WAIS Water standard ($n = 31$). In addition to the WDC samples, we measured $^{17}O_{excess}$ on a limited number of Holocene age and glacial age ice core samples from the Taylor Dome and Siple Dome ice cores using the same methods. The δ^{18}O and δD on the WDC were measured at a resolution of 0.5 m with a Picarro L1102i using cavity ring down spectroscopy and then normalized to the VSMOW-SLAP scale [*WAIS Divide Project Members*, 2013]. The precision of δ^{18}O and δD are 0.09‰ and 0.59‰, respectively, and the propagated error for d_{excess} and d_{ln} values is 0.60‰.

To eliminate interlaboratory differences among published data resulting from different calibration methods, we normalized all previously reported δ^{17}O and δ^{18}O values to the VSMOW-SLAP scale using SLAP $\delta^{18}O = -55.5$‰ and $^{17}O_{excess} = 0$ per meg, following *Schoenemann et al.* [2013]. Note that after VSMOW-SLAP normalization, some values, particularly those far removed from VSMOW, will be different than reported in the original published work. We provide all original data and data normalized to VSMOW-SLAP in Data S1 in the supporting information. In the case of the Vostok record from East Antarctica, calibration discrepancies have been noted between the two laboratories that performed the measurements, Le Laboratoire des Sciences du Climat et l'Environnement (LSCE) and Institute of Earth Sciences (IES), Hebrew University of Jerusalem [*Winkler et al.*, 2012; *Landais et al.*, 2012b; *Risi et al.*, 2013]. Long-term repeated measurements show that surface snow at Vostok is ~3 per meg, about 24 per meg lower than at WAIS Divide [*Schoenemann et al.*, 2013]. In comparing the Vostok record of $^{17}O_{excess}$ with that from WDC and other ice cores, we therefore apply an offset of −24 per meg from the mean of the VSMOW-SLAP-normalized data from *Landais et al.* [2008]. This is consistent with measurements of precipitation samples at Vostok, performed at both LSCE and IES [*Landais et al.*, 2012a].

2.1. Model Simulations

To aid interpretation of the $^{17}O_{excess}$ data, we use the European Center Hamburg atmospheric general circulation model, ECHAM4.6 [*Roeckner et al.*, 1996]. As used here, ECHAM4.6 has 19 vertical levels and a horizontal resolution of T42 (2.8° by 2.8°). We modified the water isotope module [*Hoffmann et al.,* 1998] for ECHAM4.6 by adding an implementation for $^{17}O_{excess}$ and by using the most up-to-date fractionation factors for the water isotopologues.

Equilibrium fractionation factors for deuterium ($^2\alpha_{eq} = (HD^{16}O)_l/(H_2{}^{16}O)_v$) and oxygen-18 ($^{18}\alpha_{eq} = (H_2{}^{18}O)_l/(H_2{}^{16}O)_v$) are calculated using the original temperature-dependent values from *Majoube* [1971] for $T > 273$ K, where l = liquid and v = vapor:

$$^2\alpha^{eq}_{l-v} = \exp\left(52.612\times10^{-3} - 76.248\ /T + 24844/T^2\right) \quad (4)$$

$$^{18}\alpha^{eq}_{l-v} = \exp\left(-2.0667\times10^{-3} - 0.4156/T + 1137/T^2\right) \quad (5)$$

The most important update is for ice/vapor equilibrium fractionation for temperatures between 233 K and 273 K from *Ellehøj et al.* [2013]:

$$^2\alpha^{eq}_{i-v} = \exp\left(0.2133 - 203.10/T + 48888/T^2\right) \quad (6)$$

$$^{18}\alpha^{eq}_{i-v} = \exp\left(0.0831 - 49.192/T + 8312.5/T^2\right) \quad (7)$$

$$^{17}\alpha^{eq}_{i-v} = \left(^{18}\alpha^{eq}_{i-v}\right)^{0.529} \quad (8)$$

For $(H_2{}^{17}O)_l/(H_2{}^{16}O)_v$, the equilibrium fractionation factors are calculated as $^{17}\alpha_{eq} = (^{18}\alpha_{eq})^{0.529}$ for temperatures both above and below 273 K [*Barkan and Luz*, 2005]. The kinetic fractionation factors for the molecular diffusivity of deuterium ($^2\alpha_{diff}$) include the temperature-dependent linear approximation from *Luz et al.* [2009] where the relationship between diffusive fractionations of hydrogen and oxygen is:

$$\varphi_{diff} = \left(^2\alpha_{diff} - 1\right)/\left(^{18}\alpha_{diff} - 1\right) \quad (9)$$

and the linear approximation of the temperature dependence of φ_{diff} is given by

$$\varphi_{diff(T)} = 1.25 - 0.02T\ (T\ \text{in}\ ^\circ\text{C}) \quad (10)$$

For the molecular diffusivity of $H_2{}^{18}O$ and $H_2{}^{17}O$, we use $^{18}\alpha_{diff} = D(H_2{}^{18}O)/D(H_2{}^{16}O) = 1.0096$ and $^{17}\alpha_{diff} = (^{18}\alpha_{diff})^{0.518}$ [*Barkan and Luz*, 2007; *Luz and Barkan*, 2010]. The value for $^{18}\alpha_{diff}$ was determined from water vapor samples collected over the open ocean, incorporating the influences of wind speed and molecular turbulence [*Uemura et al.*, 2010]. We note that this value is somewhat higher than values derived from experimental estimates by *Merlivat and Jouzel* [1979] ($^{18}\alpha_{diff} = 1.007$ for low wind speeds, 1.003–1.005 for rough regimes), which have frequently been used in earlier modeling work.

During snow formation, the kinetic fractionation between vapor and liquid water or ice is calculated as

$$\alpha_{kin} = \frac{S}{1 + \alpha_{eq}\left(\frac{D}{D^*}\right)(S-1)} \quad (11)$$

where S is the supersaturation parameter, following *Jouzel and Merlivat* [1984]. The effective fractionation factor is then given by $\alpha_{eff} = \alpha_{eq}\alpha_{kin}$. The supersaturation parameter, S, is assumed to be linearly related to cloud temperature (T). The diffusion constants D and D^* represent the diffusion constants for the light and heavy isotopologue, respectively. The supersaturation dependence on condensation temperature is defined by $S = a - bT$, with T in degrees Celsius and where a and b are empirical constants. We use $a = 1$ and vary b from 0.002 to 0.007, which covers the range of values used previously in both intermediate complexity isotope models and general circulation model (GCM) studies to capture observed Antarctic d_{excess} variability [*Kavanaugh and Cuffey*, 2003; *Schmidt et al.*, 2005; *Risi et al.*, 2010b; *Werner et al.*, 2011; *Landais et al.*, 2012b].

In the GCM experiments, the ocean surface water $\delta^{18}O$ and δD are set to 0‰, while $^{17}O_{excess}$ is set to −5 per meg. *Luz and Barkan* [2010] measured seawater $^{17}O_{excess}$ values ranging from −15 to 5 per meg; however, none of these measurements were made southward of 32°S, providing little constraint on seawater $^{17}O_{excess}$ for the Southern Ocean and midlatitude moisture sources. Initial conditions for atmospheric water vapor are set to 20 per meg, but results are insensitive to this value since the model water vapor quickly approaches

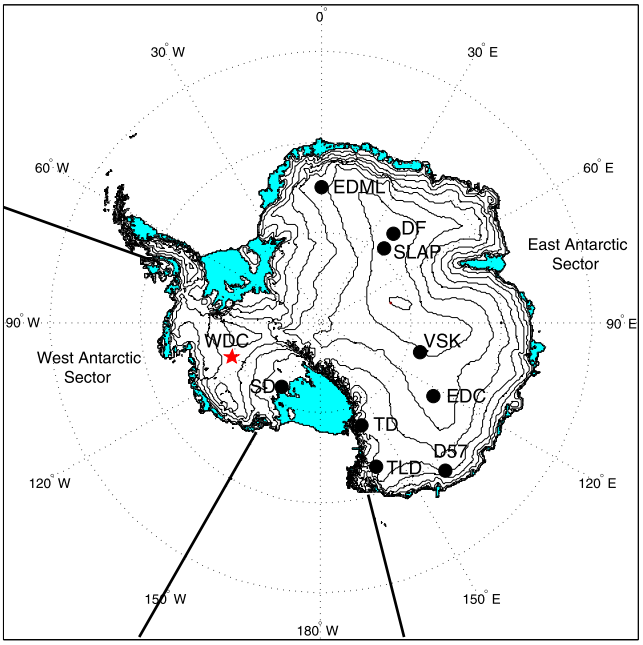

Figure 1. Map of Antarctic ice core locations and surface snow data. The West Antarctic Ice Sheet Divide ice core (WDC) is marked by the red star. The relevant sites discussed throughout the text include: Siple Dome (SD), Taylor Dome (TD), Talos Dome (TLD), European Project for Ice Coring in Antarctica (EPICA) Dome C (EDC), Vostok (VSK), Dome Fuji (DF), Plateau Station (SLAP water), EPICA Dronning Maud Land (EDML), and D57. The West Antarctic sector spans from 70°W to 150°W and the East Antarctic sector spans from 165°E to 70°W. All locations indicated above are the same throughout the following figures.

equilibrium with the ocean. *Uemura et al.* [2010] found $^{17}O_{excess}$ vapor measurements in the Southern Ocean near Antarctica (60–65°S) ranged from −8 to 19 per meg; the higher value is consistent with our GCM simulations.

To simulate present-day precipitation-weighted $\delta^{18}O$, d_{ln}, d_{excess}, and $^{17}O_{excess}$, we initialized the ECHAM4.6 atmospheric general circulation model with modern boundary conditions (preindustrial greenhouse gas concentrations, modern ice sheet topography, and orbital parameters). We prescribed a climatological seasonal sea surface temperature (SST) cycle to obtain the model's mean climate. A second control using an Atmospheric Model Intercomparison Project-style configuration (forced by historical ERA-Interim/ERA-40 SST data) for a 30 year period showed no significant difference in the mean. As noted above, a range of supersaturation sensitivities to temperature, as used in previously published model studies [*Schmidt et al.*, 2005; *Risi et al.*, 2010a; *Winkler et al.*, 2012; *Landais et al.*, 2012a; *Risi et al.*, 2013], was evaluated.

To simulate precipitation-weighted $\delta^{18}O$, d_{ln}, d_{excess}, and $^{17}O_{excess}$ for the Last Glacial Maximum (LGM, 21 ka), we prescribed boundary conditions following the Paleoclimate Modeling Intercomparison Project (PMIP II) [*Braconnot et al.*, 2007]: LGM ice sheet topography (Ice-5G) [*Peltier*, 2004], solar insolation [*Berger*, 1978], CO_2 concentration of 185 ppmv, and SST output data from an LGM experiment of the coupled ocean-atmosphere model CCSM3 [*Otto-Bliesner et al.*, 2006]. As for the modern simulations, we used a range of supersaturation sensitivities. Each experiment consisted of 30 year integrations where only the last 20 years are used. In addition to the "LGM" experiments, we performed "LGM-cold" simulations in which a uniform 4°C global decrease to the LGM sea surface temperature field is applied, in order to better match the high-latitude temperatures estimated from Antarctic ice core reconstructions.

To complement the LGM and LGM-cold experiments, in which the change in SST and sea ice boundary conditions is found to play a significant role in the resulting $\delta^{18}O$, d_{ln}, d_{excess}, and $^{17}O_{excess}$ fields, we performed another set of experiments (Extend-Ice) that use modern boundary conditions but with extended sea ice. We prescribe an amplified sea ice seasonality, as supported by *Collins et al.* [2012] for the LGM. In winter, the edge of sea ice is expanded ~10° north from the edge of the present-day model (July, August, and September, JAS) sea ice climatology, while in the summer (January, February, and March, JFM) the sea ice extent is equal to present-day. In the transition seasons (October, November, and December (OND) and April, May, and June (AMJ)), we extend the sea ice edge by ~5°.

To make comparisons of the isotopic records and model results, we account for the change in $\delta^{18}O$ and δD composition of the ocean during the glacial period resulting from the buildup of continental ice sheets. These seawater corrections have a considerable influence on the d_{excess} records and are therefore necessary in order to interpret the glacial-interglacial d_{excess} changes [*Jouzel et al.*, 2003; *Stenni et al.*, 2010b]. We find that the d_{ln} definition of d_{excess} (following *Uemura et al.* [2012]) reduces the large impact of the isotopic seawater correction

Table 1. Present-Day (PD) δD, δ^{18}O, d_{excess}, d_{ln}, and $^{17}O_{excess}$ Isotopic Measurements From Snow or Ice Core Samples[a]

Ice Core	Sample Type	PD δD (‰)	PD δ^{18}O (‰)	PD d_{excess} (‰)	PD d_{ln} (‰)	EH $^{17}O_{excess}$ (per meg) VSMOW-SLAP	PD $^{17}O_{excess}$ (per meg) VSMOW-SLAP
WDC[e]	ice core	−264.35	−33.46	3.32	14.24	29	25
WW UW Isolab[f]	snow	−267.44	−33.82	2.64	13.29	––	27
Siple Dome[g]	ice core	−205.38	−26.16	3.89	14.63	––	21
Taylor Dome[h]	ice core	−315.03	−40.17	4.99	14.87	17	––
D57[i]	snow	−258.14	−32.63	2.90	13.76	––	20
SLAP (Plateau Sta.)[j]	snow	−428.00	−55.50	16.00	17.94	––	0
VW UW Isolab[j]	snow	−438.57	−56.56	13.91	12.50	––	3
Vostok[l]	ice core	−441.28	−57.09	15.44	14.28	6[c]	2[b], −8[c]
Dome C[m]	ice core	−396.66	−50.73	9.16	12.97	19[b]	23[c]
Talos Dome[n]	ice core	−285.62	−36.19	3.92	14.61	0[b]	––
Dome F[o]	ice core	−426.01	−55.04	14.32	15.65	––	−6[c]
EDML[p]	ice core	−353.89	−44.82	4.69	11.54	8[d]	––

[a]The present-day is defined as the past 2 kyr average, except for Dome C δ^{18}O, δD (2–1.2 ka), and Siple Dome $^{17}O_{excess}$ (2–1 ka) due to lack of available data. All $^{17}O_{excess}$ data normalized to VSMOW-SLAP scale as in *Schoenemann et al.* [2013], except EDML $^{17}O_{excess}$ (see supporting information). Note, that for snow, the present-day consists of multiple years of accumulation to provide the annual average reference water value (e.g., not 2 kyr). Early Holocene (EH = 12–9 ka), except for Taylor Dome $^{17}O_{excess}$ (6–2 ka) due to lack of available ice core data. The d_{ln} values are calculated using equation (3), as in *Uemura et al.* [2012, equation (A1)].
[b]$^{17}O_{excess}$ measurements performed at LSCE.
[c]$^{17}O_{excess}$ measurements performed at IES.
[d]$^{17}O_{excess}$ unpublished from *Risi et al.* [2013], not VSMOW-SLAP normalized.
[e]*WAIS Divide Project Members* [2013] and this study.
[f]Updated from *Schoenemann et al.* [2013] with more data.
[g]*Brook et al.* [2005] and this study.
[h]*Steig et al.* [1998b] and this study.
[i]This study (reference water from LSCE).
[j]*Schoenemann et al.* [2013].
[k]*Schoenemann et al.* [2013].
[l]*Vimeux et al.* [2001] and *Landais et al.* [2008, 2012a].
[m]*EPICA Community Members* [2004], *Stenni et al.* [2004], and *Winkler et al.* [2012].
[n]*Stenni et al.* [2010a], B. Stenni, (personal communication, 2013), Talos Dome (unpublished d_{excess} data), and *Winkler et al.* [2012].
[o]*Fujita and Abe* [2006], and *Luz and Barkan* [2010].
[p]*EPICA Community Members* [2006], *Stenni et al.* [2010b], *Winkler et al.* [2012], and *Risi et al.* [2013].

on d_{excess}. Seawater-corrected d_{ln} and d_{excess} ice core data are referred-to throughout as $d_{ln\ corr}$ and $d_{xs\ corr}$. The seawater correction for $^{17}O_{excess}$ results in a negligible change (<0.5 per meg), and therefore, we leave $^{17}O_{excess}$ uncorrected.

3. Results

3.1. Ice Core Data

Table 1 compares data from present-day surface snow and Holocene ice at WAIS Divide, Taylor Dome, and Siple Dome (Figure 1), with previously published data from ice core sites in East Antarctica [*Vimeux et al.*, 2001; *Landais et al.*, 2008; *Masson-Delmotte et al.*, 2008; *Stenni et al.*, 2010a; *Uemura et al.*, 2012; *Winkler et al.*, 2012]. For the ice core records, "present-day" is defined as the average value of the past 2 kyr except for $^{17}O_{excess}$ at Taylor Dome (6–2 ka) and EPICA Dome C (EDC) (2–1.2 ka) due to limited availability of samples.

In Figures 2, 3, and 4, we compare $^{17}O_{excess}$ and δ^{18}O for WAIS Divide with the results from Taylor Dome, Siple Dome, Vostok, Talos Dome, and EDC. The WDC $^{17}O_{excess}$ measurements cover from ~25 ka to the present. The WDC data provide the highest resolution available measurements of $^{17}O_{excess}$ from the LGM through the entire Holocene. The minimum resolution is four samples per thousand years. Both the individual measurements (sample mean) and 1σ standard deviation are shown for the WDC record, along with a Monte Carlo average cubic spline and 1σ (6 per meg) standard deviation envelope following the methods given in *Schmitt et al.* [2012]. In Figure 3, we show $^{17}O_{excess}$ measurements of Taylor Dome and Siple Dome for the LGM and some Holocene periods. Included are previously published δ^{18}O records of Taylor Dome and Siple Dome each on their published timescales [*Steig et al.*, 2000; *Brook et al.*, 2005]. For consistency with previous $^{17}O_{excess}$ studies [*Landais et al.*, 2008; *Winkler et al.*, 2012], we compare the records for LGM (25–20 ka) and Early Holocene (12–9 ka) time periods.

Our results show that, in general, present-day West Antarctic ice core $^{17}O_{excess}$ samples have elevated mean annual values compared to those of the East Antarctic interior. This pattern also appears to hold throughout

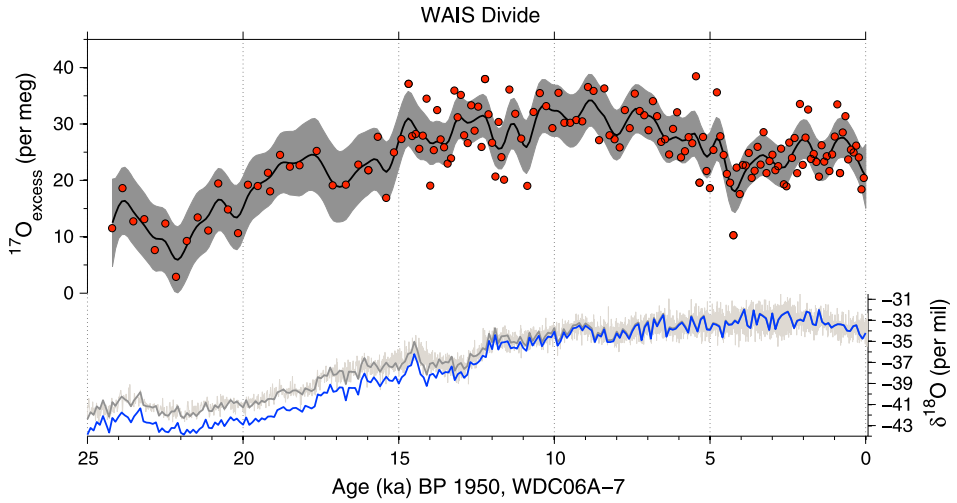

Figure 2. WDC record of $^{17}O_{excess}$ (black line = Monte Carlo Cubic Spline Average, gray band = 1σ standard deviation) and $\delta^{18}O$ (light gray = original data, dark gray = 200 year average, and blue = 200 year average seawater corrected) on the WDC06A-7 timescale. We follow the Monte Carlo Averaging (MCA) methods used by *Schmitt et al.* [2012]. The MCA is composed of 4000 randomly distributed iterations, with a 100 year resolution, and a cutoff period of 1000 years. All data are included in the 1σ envelope of 6 per meg [see *Schmitt et al.*, 2012].

the Holocene. The LGM to EH change in $^{17}O_{excess}$ at WAIS Divide is 17 per meg, very similar to that at Vostok (22 per meg) (Table 2). The $^{17}O_{excess}$ change between LGM and EH at WAIS Divide appears to occur in two steps, with a first increase beginning around 22 ka, and a second, marked increase at ~15 ka. There is a short decrease during the Antarctic Cold Reversal (14.5 to 11.9 ka), followed by a period (11.5–9.5 ka) of elevated

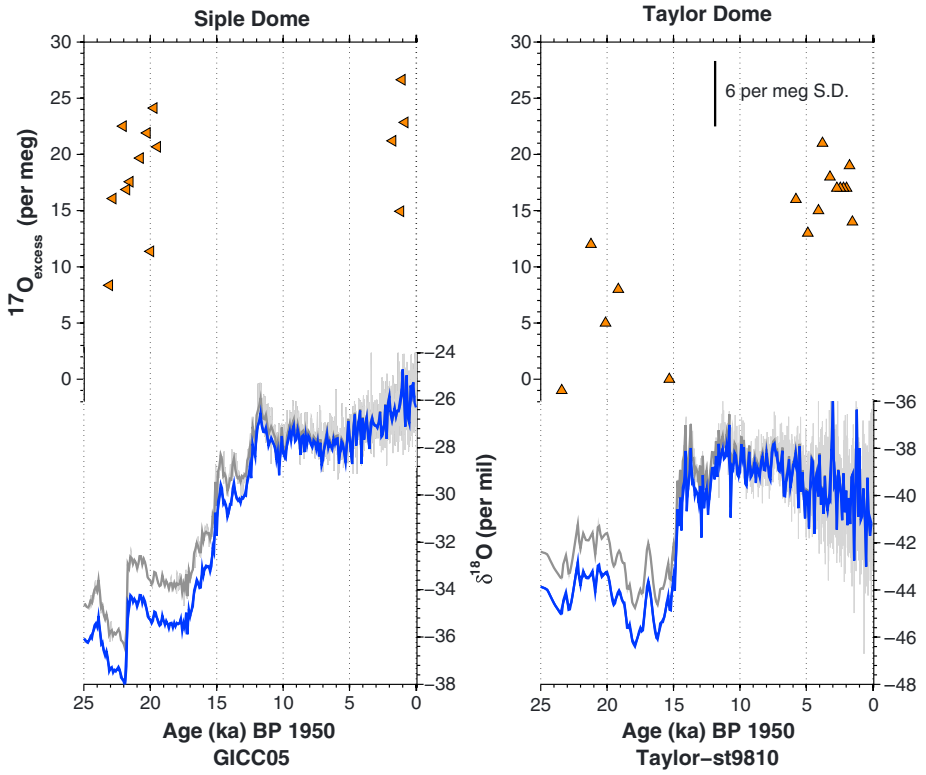

Figure 3. Record of $^{17}O_{excess}$ and $\delta^{18}O$ for Siple Dome for LGM and late Holocene (2–1 ka) on the GICC05 age scale [*Brook et al.*, 2005] and $^{17}O_{excess}$ and $\delta^{18}O$ for Taylor Dome for LGM and mid-Holocene (6–2 ka). Note that the Taylor Dome timescale used is *st9810,* which has large age errors in the LGM period [*Steig et al.*, 2000].

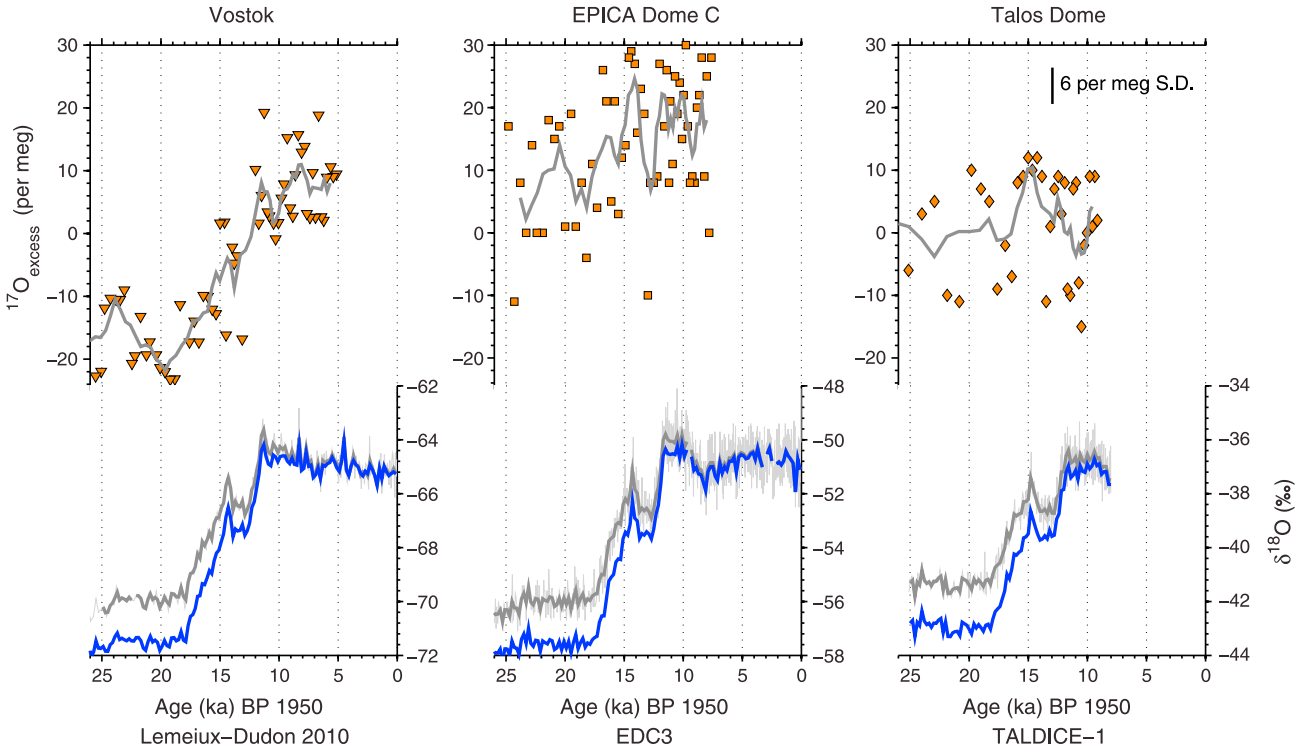

Figure 4. East Antarctic ice core records spanning the LGM (25–20 ka) to Early Holocene (12–9 ka) from Vostok, Dome C, and Talos Dome for $^{17}O_{excess}$ (orange, gray 5 point running mean) [*Landais et al.*, 2008; *Winkler et al.*, 2012], and $\delta^{18}O$ (light gray = original data, dark gray = 200-year average, and blue = 200 year average seawater corrected) normalized to the VSMOW-SLAP scale. Vostok $^{17}O_{excess}$ record has been shifted down based on UW IsoLab WW − VW difference of 24 per meg. The $^{17}O_{excess}$ data are presented on their originally published age scales: Dome C on EDC3, Talos Dome on TALDICE-1, and for Vostok, the $\delta^{18}O$ data have been transferred to the Lemiuex-Dudon 2010.

Table 2. Change in $\delta^{18}O$, δD, d_{excess}, and d_{ln} From the Last Glacial Maximum (LGM) to Early Holocene (EH) and Present-Day (PD) for Seawater Isotopic Corrected Ice Core Data ($_{corr}$)[a]

Ice Core Site	LGM-EH $\delta^{18}O_{corr}$ (‰)	LGM-PD $\delta^{18}O_{corr}$ (‰)	LGM-EH $d_{xs\ corr}$ (‰)	LGM-PD $d_{xs\ corr}$ (‰)	LGM-EH $d_{ln\ corr}$ (‰)	LGM-PD $d_{ln\ corr}$ (‰)	LGM $^{17}O_{excess}$ (per meg)	EH $^{17}O_{excess}$ (per meg)	LGM-EH $^{17}O_{excess}$ (per meg)
WDC[f]	−8.04	−9.44	−0.76	−0.67	−4.89	−5.16	12	29	−17
Siple Dome[g]	−8.27	−9.80	0.12	−1.05	−0.79	−2.24	18	21[e]	−3
Taylor Dome[h]	−5.23	−3.55	−2.65	−3.61	−7.06	−7.98	6	17[e]	−11
Vostok[i,c]	−6.96	−5.66	5.02	3.08	−5.67	−7.08	−16	6	−22
EPICA Dome C[j,b]	−6.95	−6.74	2.07	2.00	−7.77	−7.82	7	19	−12
Talos Dome[k,b]	−5.86	−6.84	−3.28	−3.67	−8.24	−9.24	−1.5	0	−1.5
Dome F[l]	−6.89	−6.20	4.86	4.58	−4.60	−4.19	––	––	––
EDML[m]	−6.89	−7.00	2.95	2.57	−3.13	−4.00	6[d]	8[d]	−2

[a]LGM (20–25 ka), EH (12–9 ka), and PD (2–0 ka), except for EDC $\delta^{18}O$, δD, and d_{excess} (2–1.2 ka). All $^{17}O_{excess}$ data normalized to VSMOW-SLAP scale as in *Schoenemann et al.* [2013], except EDML $^{17}O_{excess}$.
[b]$^{17}O_{excess}$ measurements performed at LSCE.
[c]$^{17}O_{excess}$ measurements performed at IES.
[d]$^{17}O_{excess}$ unpublished in *Risi et al.* [2013], from *Winkler et al.* [2012].
[e]Siple $^{17}O_{excess}$ PD = (2-1 ka), Taylor $^{17}O_{excess}$ EH = (6–2 ka).
[f]*WAIS Divide Project Members* [2013] and this study.
[g]*Brook et al.* [2005] and this study.
[h]*Steig et al.* [1998b] and this study.
[i]*Vimeux et al.* [2001], *Landais et al.* [2008, 2012a],and *Risi et al.* [2013].
[j]*EPICA Community Members* [2004], *Stenni et al.* [2004, 2010b], *Winkler et al.* [2012].
[k]*Stenni et al.* [2010a]; B. Stenni (personal communication , 2013), Talos Dome (unpublished d_{excess} data), and *Winkler et al.* [2012].
[l]*Fujita and Abe* [2006].
[m]*EPICA Community Members* [2006], *Stenni et al.* [2010b], *Winkler et al.* [2012], and *Risi et al.* [2013].

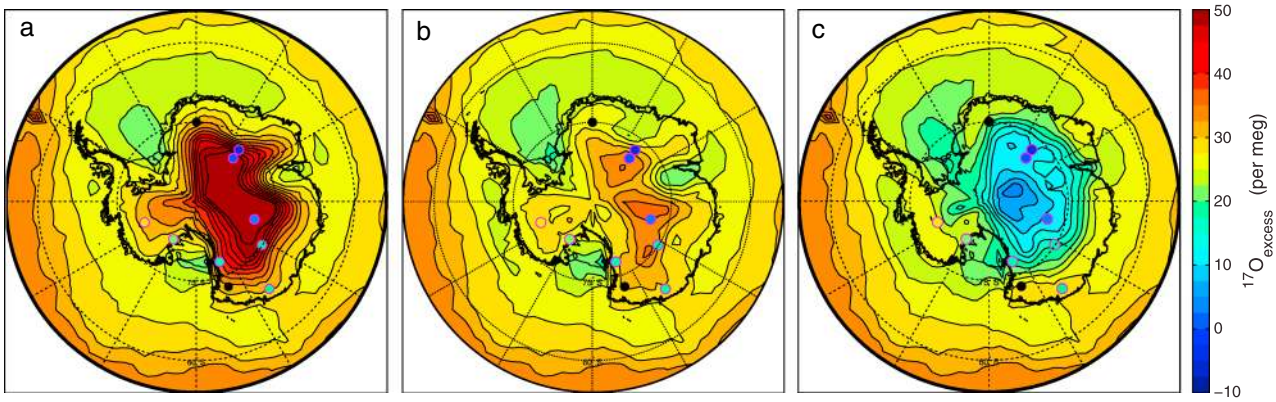

Figure 5. (a) Present-day spatial gradient of modeled $^{17}O_{excess}$ using supersaturation parameterization of $S = 1 - 0.002\,T$, (b) $S = 1 - 0.004\,T$, and (c) $S = 1 - 0.007\,T$ from ECHAM4.6, compared to the present-day $^{17}O_{excess}$ ice core data normalized to VSMOW-SLAP as in *Schoenemann et al.* [2013] from Table 1. Note, the model output for all three panels has been offset by +20 per meg for straightforward comparison with the ice core values.

values in the early Holocene. The early Holocene maximum is followed by a long-term $^{17}O_{excess}$ decrease toward the present (~1 per meg/ka); such a long-term decrease has not previously been identified in Antarctic ice cores, which generally have not included data more recent than the mid-Holocene.

Together, the multiple data sets show a clear spatial pattern to the change in $^{17}O_{excess}$ between LGM and Holocene periods, with more coastal sites showing very little change, and sites in the interior showing greater change. At the low elevation coastal site of Siple Dome, there is no measurable change in $^{17}O_{excess}$, similar to the lack of significant change at Talos Dome. At Taylor Dome, $^{17}O_{excess}$ increases by 11 per meg from LGM to the mid-Holocene, comparable to the change at Dome C.

3.2. Model-Data Comparison

3.2.1. Present-Day Conditions

Figure 5 compares the spatial distribution of present-day $^{17}O_{excess}$ measurements with the modeled spatial pattern, for different temperature-dependent parameterizations of the supersaturation value ($S = a - bT$;

Table 3. Site Characteristics of Ice Core Locations for the Present-Day Compared to ECHAM4.6 GCM Control Simulation[a]

	Site Observations						Model	
Location	Latitude (S)	Longitude	Elevation (m MSL)	Distance to Coast (km)	Current Accumulation Rate (mm w.e./yr)	Mean Annual Surface Temperature (°C)	ECHAM 4.6 Accumulation Rate (mm w.e./yr)	ECHAM4.6 Mean Annual Surface Temperature (°C)
WDC[b]	−79.47	−112.08	1766	585	220.0	−28.5	437.2	−23.0
Siple Dome[c]	−81.67	−148.82	621	470	106.1	−24.5	185.1	−25.2
Taylor Dome[d]	−77.79	158.72	2365	120	47.4 to 66.3	−37, −41	41.0	−35.5
D57[e]	−68.46	140.00	2000	200	––	––	521.4	−25.5
Plateau Station[f]	−79.25	40.55	3625	1100	25.4	−56.4	21.3	−50.0
Vostok[g]	−78.47	106.87	3488	1260	21.8	−57	15.2	−52.3
Dome C[h]	−75.1	123.35	3233	870	26.9	−54.5	15.7	−49.3
Talos Dome[i]	−72.81	159.18	2318	250	80.5	−41, −43	168.2	−27.1
Dome F[j]	−77.32	39.70	3810	1000	25 to 30	−54.8, −57.7	14.6	−50.0
EDML[k]	−75.00	0.07	2892	529	60.6	−43.2	51.0	−34.8

[a] Model output for the 2.8° × 2.8° grid surrounding the ice core latitude-longitude.
[b] *WAIS Divide Project Members* [2013] and *Orsi et al.* [2012].
[c] *Brook et al.* [2005].
[d] *Steig et al.* [1998b, 2000].
[e] *Legrand and Delmas* [1985].
[f] *Radok and Lile* [1977].
[g] *Petit et al.* [1999].
[h] *EPICA Community Members* [2004], *Stenni et al.* [2004], and *Jouzel et al.* [2007].
[i] *Frezzotti et al.* [2004] and *Stenni et al.* [2010a].
[j] *Watanabe et al.* [2003], *Motoyama et al.* [2005], and *Fujita and Abe* [2006].
[k] *EPICA Community Members* [2006].

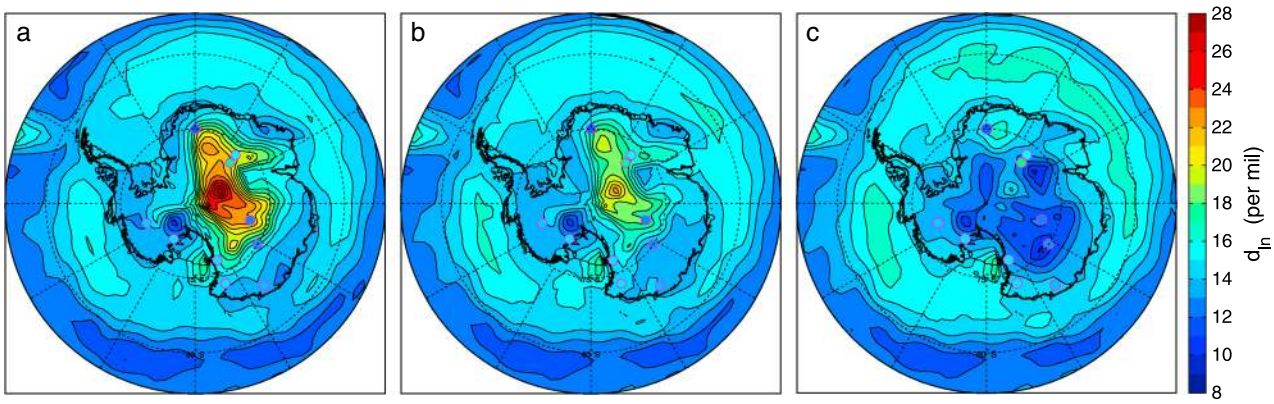

Figure 6. (a) Present-day spatial gradient of d_{ln} using supersaturation parameterization of $S = 1 - 0.002\,T$, (b) $S = 1 - 0.004\,T$, and (c) $S = 1 - 0.007\,T$ from ECHAM4.6, and present-day ice core d_{ln} data from Table 1.

$a = 1$; $b = 0.002$, 0.004, 0.007). To make straightforward comparisons between the spatial patterns in the data and modeling results, we offset the model output (+20 per meg, +4‰, and +3‰) such that the model WAIS Divide grid cell $^{17}O_{excess}$, d_{ln}, and d_{excess} values match the real WDC values (27 per meg, 13‰, and 3‰, respectively).

We find that the best fit for the $^{17}O_{excess}$ spatial pattern is obtained when using large values for *b,* reflecting a strong sensitivity of supersaturation to temperature. As shown in Figure 5, using $b = 0.007$, the modeled spatial pattern captures the higher $^{17}O_{excess}$ values found in West Antarctica (WAIS Divide and Siple Dome) and also shows relatively high $^{17}O_{excess}$ along the coastal margins of East Antarctica but low values in the central East Antarctic plateau. In contrast, using moderate and low sensitivity of supersaturation to temperature ($b = 0.004$ and 0.002) results in an overestimation of $^{17}O_{excess}$ values in East Antarctica and fails to reproduce the strong negative spatial gradient observed in present-day $^{17}O_{excess}$ between the coast and the East Antarctica interior. Indeed, even the $b = 0.007$ model experiments overestimate the $^{17}O_{excess}$ values found at Vostok, Plateau Station (SLAP), and Dome F, relative to those at WAIS Divide. This could suggest an even greater sensitivity of supersaturation to temperature; however, the magnitude of this difference is also a function of model resolution and the model bias that tends to produce temperatures over East Antarctica that are too warm (Table 3) [*Hoffmann et al.*, 1998; *Schmidt et al.*, 2005; *Helsen et al.*, 2007; *Werner et al.*, 2011].

Comparison of present-day d_{ln} data with the model results is shown in Figure 6. We find that, as for $^{17}O_{excess}$, the best overall agreement between d_{ln} data and model simulations occurs with a relatively high sensitivity of supersaturation to temperature (e.g., $b = 0.007$). We note that most previous model simulations of d_{excess} in Antarctica have used lower sensitivity ($b = 0.002$ to 0.0045) to match present-day data. However, most of this earlier work was based on fractionation factors for δD and δ^{18}O that were poorly constrained at low temperature. Our results show that, when the most up-to-date fractionation factors [*Luz et al.*, 2009; *Ellehøj et al.*, 2013] are used, the d_{ln} data are consistent with the greater sensitivity required by the $^{17}O_{excess}$ data. Lower sensitivities to supersaturation result in very high d_{ln} values in the East Antarctic interior, inconsistent with the data (Table 1 and Figures 6a and 6b).

3.2.2. LGM to Holocene Change

We now consider model-data comparison for the LGM period and for the magnitude of the LGM to Holocene transition. We use results from the present-day simulations as an approximation of early Holocene conditions. The limited data available suggest that Early Holocene (EH) $^{17}O_{excess}$ values are generally elevated relative to present, so that the model calculation of the LGM minus present-day may tend to underestimate the total isotopic LGM to EH change. Note that, taken at face value, the published data of *Landais et al.* [2008] compared with those of *Landais et al.* [2012a] imply a ~30 per meg decline in $^{17}O_{excess}$ since the Early Holocene. Given the calibration discrepancies noted above, and the small $^{17}O_{excess}$ difference between EH and present-day at both Dome C and WAIS Divide, we think this is unlikely. Indeed, assuming that Vostok is similar to Dome C in having only a modest difference between EH and present-day is consistent with the offset to the published Vostok

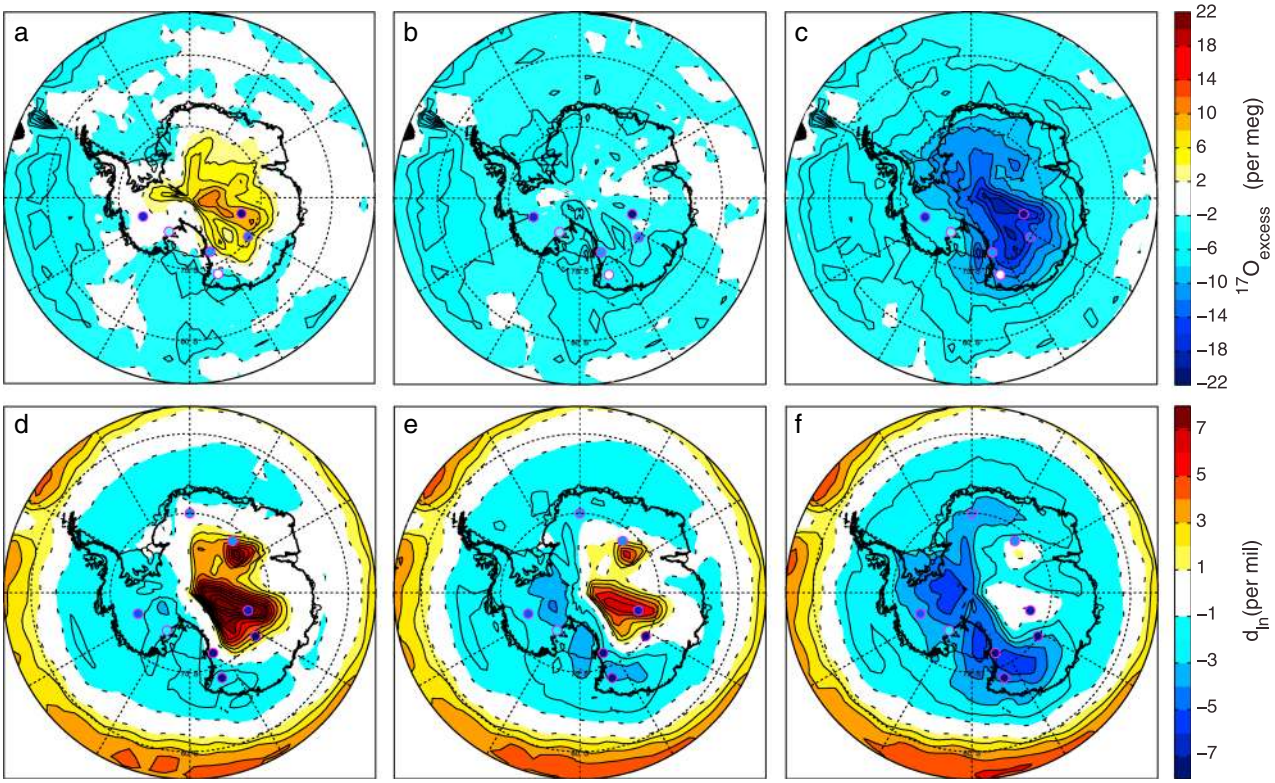

Figure 7. Model simulations for the LGM (21 ka) minus PD (0 ka) performed by ECHAM4.6 to determine (a–c) $^{17}O_{excess}$ and (d–f) d_{ln} sensitivity to all three supersaturation values ($S = 1 - 0.002\,T$ in Figures 7a and 7d, $S = 1 - 0.004\,T$ in Figures 7b and 7e, and $S = 1 - 0.007\,T$ in Figures 7c and 7f), compared with the LGM-EH change in $^{17}O_{excess}$ and $d_{ln\ corr}$ ice core data (Table 2). All experiments were run at T42 (2.8° by 2.8°) resolution.

data suggested by available interlaboratory comparisons. This assumption has no impact on the magnitude of the glacial-interglacial change.

All model comparisons hereafter are "Experiment" minus "Control" (e.g., LGM minus present-day). In Figure 7 we show the spatial pattern of $^{17}O_{excess}$ and d_{ln} change between LGM and present-day model simulations, for different supersaturation parameterizations. As for the modern spatial pattern, the best reproduction of the observed spatial pattern of LGM to EH $^{17}O_{excess}$ change is achieved with $b = 0.007$. Using this high sensitivity of supersaturation to temperature captures the large decrease (22 per meg) in $^{17}O_{excess}$ values at Vostok during the LGM, while also correctly simulating the smaller (~12 per meg) $^{17}O_{excess}$ decreases observed at Dome C and Taylor Dome. At WAIS Divide, the high-sensitivity LGM simulation underestimates the full magnitude of the glacial to interglacial $^{17}O_{excess}$ change but correctly predicts the sign. In contrast, lower values of b result in LGM $^{17}O_{excess}$ values that are of incorrect sign and higher than present in the East Antarctic interior (for example, an LGM minus EH change of +9 per meg at Vostok, opposite in sign to the observed −22 per meg change).

The same high-sensitivity value for supersaturation parameter b that best fits the $^{17}O_{excess}$ data also better captures the observed spatial pattern in $d_{ln\ corr}$ change between the LGM and present-day. The model pattern is characterized by greater, more negative d_{ln} changes in West Antarctica and coastal areas and relatively small, positive d_{ln} changes in the central East Antarctica interior. In contrast, LGM model simulations using low and moderate supersaturation sensitivities result in larger, positive d_{ln} changes in the East Antarctic interior, contrary to the negative $d_{ln\ corr}$ changes in the ice core data. The high-sensitivity ($b = 0.007$) model result shows a uniform decrease in d_{ln} values around the periphery of the continent during the LGM, which is supported by the $d_{ln\ corr}$ ice core data. The model result closely matches the magnitude of LGM to EH change at EDML and WDC, though it underestimates the LGM minus EH change in $d_{ln\ corr}$ at Vostok and Dome F.

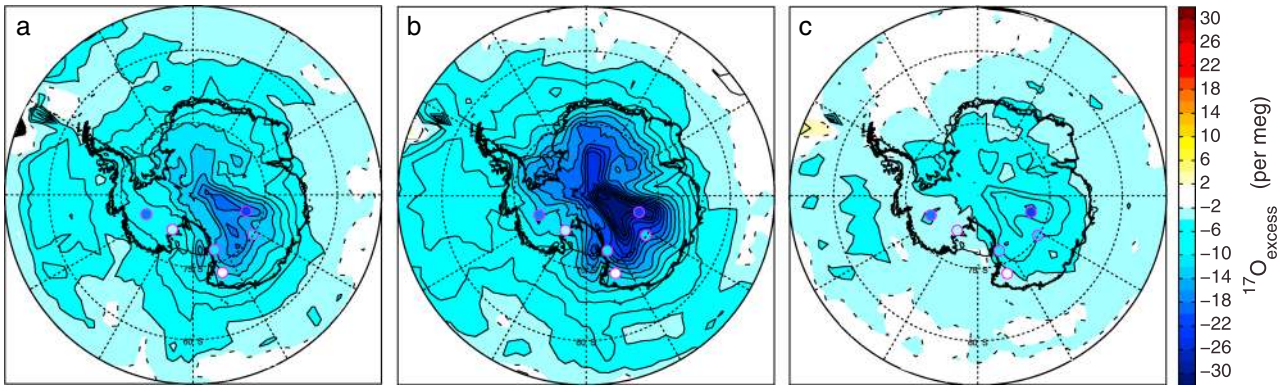

Figure 8. $^{17}O_{excess}$ spatial difference maps comparing model simulations for (a) LGM, (b) LGM-cold, and (c) Extend-Ice minus PD (0 ka), using ECHAM4.6 (GCM) with high sensitivity to supersaturation ($S = 1 - 0.007$ T). Note change in color bar scale of −32 to 32, from −22 to 22 in Figure 7.

For the case of $d_{xs\ corr}$, the low and moderate sensitivity LGM minus present-day experiments result in greatly overestimated change in $d_{xs\ corr}$ (by 4–6 ‰) in the central East Antarctic interior, while the high-sensitivity simulation achieves the spatial distribution of LGM to EH change in $d_{xs\ corr}$ most consistent with the data, characterized by lower LGM minus present-day $d_{xs\ corr}$ values in West Antarctica and coastal regions, and higher LGM minus present $d_{xs\ corr}$ values on the East Antarctic plateau (Figure S1). We emphasize that the seawater correction is such that the glacial-interglacial change of $d_{xs\ corr}$ in the East Antarctic interior is of opposite sign to that of d_{excess} [*Stenni et al.*, 2010b], and the magnitude of change is greatly reduced in West Antarctica (Figure S2). This potentially confusing change in sign is another reason why in general d_{ln} is a more useful parameter than d_{excess}.

3.2.3. Dependence on Model Boundary Conditions

The Modern and LGM model results both show that a relatively high sensitivity of supersaturation to temperature best reproduces the $^{17}O_{excess}$ data. The details of the $^{17}O_{excess}$ response depend on the model boundary conditions, particularly SST and sea ice cover. We performed two additional sets of experiments to examine the sensitivity of $^{17}O_{excess}$ to varying these boundary conditions. Here we use only $b = 0.007$, for comparison with the best results from the LGM and Modern experiments.

A recognized problem with GCMs is the difficulty in simulating cold-enough Antarctic temperatures, both in modern and LGM simulations [*Hoffmann et al.*, 2005; *Schmidt et al.*, 2005; *Masson-Delmotte et al.*, 2008; *Werner et al.*, 2011]. To assess the importance of this issue for simulating $^{17}O_{excess}$, we performed a set of "LGM-cold" model experiments, where we prescribed a global 4°C decrease to LGM SSTs. Unlike the LGM simulation, the LGM-cold model experiment produces Antarctic mean surface temperatures that are comparable to paleoclimate estimates from ice cores [*Jouzel et al.*, 2003]. The magnitude of LGM-cold minus present-day temperature change on the central East Antarctica plateau is more consistent with the ice core records at Dome F and Vostok (−8 to −12°C, respectively) than the LGM simulation but results in an unrealistically large $^{17}O_{excess}$ change in this region (Taylor Dome ~ 21, Dome C ~ 22 per meg, Vostok ~ 32 per meg) (Figure 8b). On the other hand, the LGM-cold experiment better reproduces the magnitude of LGM to Early Holocene change in $^{17}O_{excess}$ at WAIS Divide (~14 per meg).

Comparisons between the LGM-cold and LGM experiment show that in general, making the model colder produces the expected response of greater $^{17}O_{excess}$ changes in the interior resulting from even stronger kinetic fractionation due to colder temperatures. However, the pattern of $^{17}O_{excess}$ change does not directly follow the pattern of temperature change, showing that the spatial pattern of $^{17}O_{excess}$ change is not simply a linear function of temperature. An important aspect of the LGM-cold experiment is that the sea ice extent is overestimated by (~3 to 12° of latitude, as shown in Figure 9), relative to estimates of LGM sea ice extent from proxy reconstructions [*Gersonde et al.*, 2005; *Collins et al.*, 2012; *Roche et al.*, 2012]), and this may also affect the $^{17}O_{excess}$.

To examine the influence of sea ice extent on $^{17}O_{excess}$, we performed an additional experiment, "Extend-Ice," in which we use modern SST boundary conditions but prescribe amplified sea ice seasonality. In winter, we

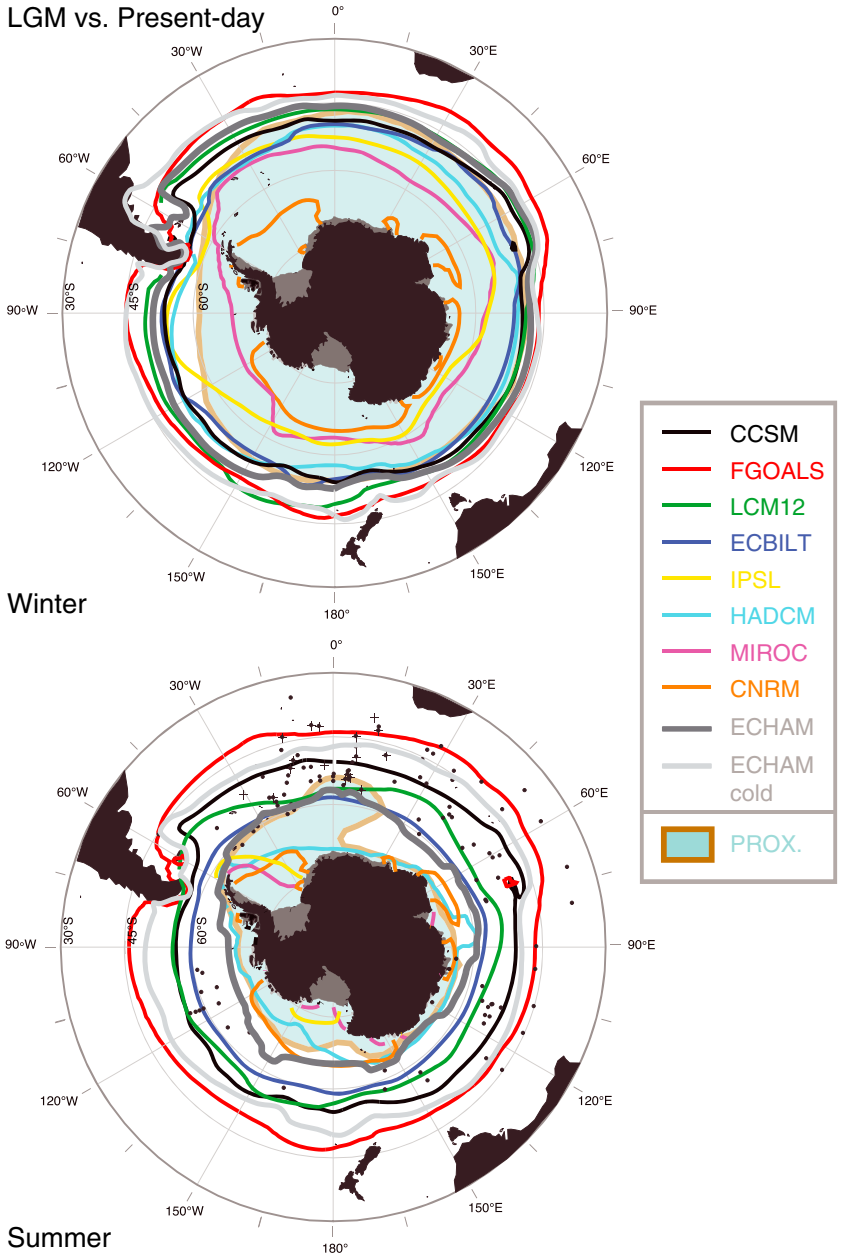

Figure 9. Comparison of LGM (dark gray) and LGM-cold (light gray) ECHAM4.6 winter and summer sea ice extent with multiple LGM GCM simulations adapted from *Roche et al.* [2012]. Maximum sea ice extent (>15 % sea ice concentration) for LGM (21 ka) compared with other GCM LGM simulations and proxy data [*Gersonde et al.*, 2005] for (top) winter and (bottom) summer.

extend the model sea ice climatology by ~10°N but keep summer sea ice extent unchanged. Between summer and winter the sea ice is prescribed to change linearly, extending ~5°N on average for both fall and spring seasons (Figure 10). Annual average results show that the extended sea ice margin results in a decrease of $^{17}O_{excess}$ over the entire Antarctic continent, with decreases of 8 to 12 per meg in the Antarctic interior over Vostok and Dome C, and a decrease at WAIS Divide of ~5 per meg, roughly half the response of the LGM simulation (Figure 8). The Extend-Ice simulations show a particularly strong decrease in $^{17}O_{excess}$ over West (~9 per meg) and East Antarctica (~14 per meg) during winter (JAS), as expected due to the prescribed winter sea ice expansion.

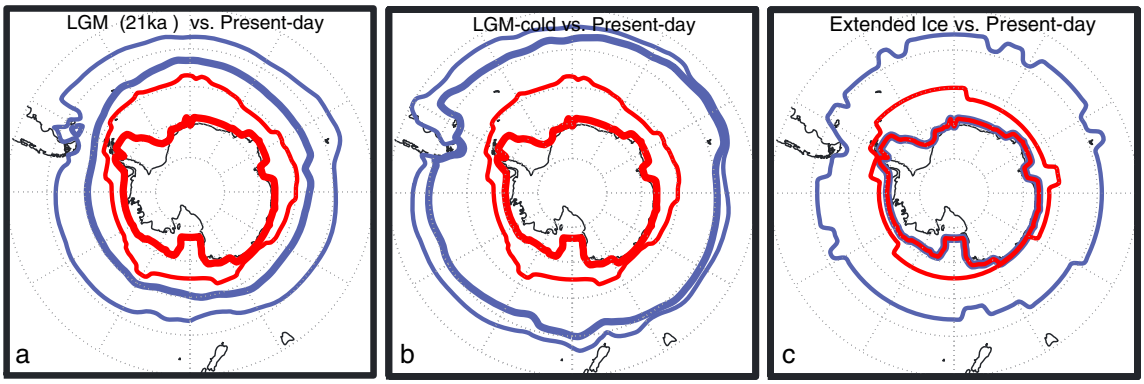

Figure 10. (a) Comparison of winter (thin) and summer (bold) sea ice extent for LGM (21 ka) (blue) versus present-day (red) in ECHAM4.6. (b) LGM-cold (21 ka minus 4°C) versus present-day. (c) Extended sea ice (modern day boundary conditions and 10°N expansion of winter-time sea ice) versus present-day. Winter and summer sea ice calculated as JAS and JFM mean.

4. Discussion

4.1. Controls on the $^{17}O_{excess}$ in Antarctic Precipitation

Interpretation of $^{17}O_{excess}$ in Antarctic ice cores has been challenging due to limited and inconsistently-calibrated data. Our findings show that there is a clear present-day spatial gradient of $^{17}O_{excess}$ across Antarctica, with higher values in the coastal and marine-influenced regions and lower values in the central East Antarctic interior. There is a similar spatial pattern to the change in $^{17}O_{excess}$ between the Last Glacial Maximum (LGM) and Early Holocene (EH) periods, with near-coastal sites showing little or no change in $^{17}O_{excess}$, while sites further inland—in both East and West Antarctica—indicate a greater magnitude of change. In the following paragraphs we discuss the implications of these results, with a focus on what matters to $^{17}O_{excess}$ in terms of climate boundary conditions. Sea ice extent emerges as a particularly important factor.

To illustrate the sensitivity of $^{17}O_{excess}$ to different model boundary conditions, we calculate the zonal annual average response of $^{17}O_{excess}$ (for $b = 0.007$), sea ice fraction, surface temperature, and rh_n versus latitude for all the model experiments (Modern, LGM, LGM-cold, and Extend-Ice). We display the West and East Antarctic sectors separately to allow for regional differences in sea ice concentration and extent (Figures 11 and 12). The gray bars highlight the latitude of maximum sea ice extent for each model experiment.

Figures 11 and 12 show that for both modern snowfall and for the LGM-EH change, the influence of supersaturation largely determines how $^{17}O_{excess}$ varies with latitude on the ice sheet. As already noted, the values used for tuning the sensitivity of supersaturation to temperature spans the range typically used in most previous work [*Hoffmann et al.*, 1998; *Schmidt et al.*, 2005; *Risi et al.*, 2010b; *Landais et al.*, 2012b], and a value of $b = 0.007$ in the standard linear parameterization provides a significantly better match to the data than lower values. That reasonably good model agreement with d_{ln} data during the present-day and LGM is also achieved with $b = 0.007$ provides further support for a strong sensitivity of supersaturation to temperature.

In contrast with the supersaturation effect, ocean surface relative humidity has a limited role in explaining the $^{17}O_{excess}$ of Antarctic precipitation. Normalized relative humidity does determine the initial $^{17}O_{excess}$ value in the marine boundary layer, and as the model results in Figures 11 and 12 illustrate, $^{17}O_{excess}$ in precipitation roughly tracks rh_n in midlatitudes, beginning to decrease as rh_n increases (when going from the equator towards the poles). However, the humidity-$^{17}O_{excess}$ relationship is decoupled at higher latitudes, as the strong dependence of $^{17}O_{excess}$ on kinetic fractionation increases in importance as colder temperatures are encountered. Indeed, the present-day latitudinal distribution of $^{17}O_{excess}$ is contrary to that expected if oceanic moisture source regions control present-day Antarctic $^{17}O_{excess}$ values. In the case of Vostok, Dome C, and Dome Fuji, for example, the dominant moisture sources are estimated to be from subtropical to midlatitude oceans [*Sodemann and Stohl*, 2009], which corresponds with lower rh_n and should therefore result in higher $^{17}O_{excess}$, whereas lower $^{17}O_{excess}$ is observed. In West Antarctica and coastal

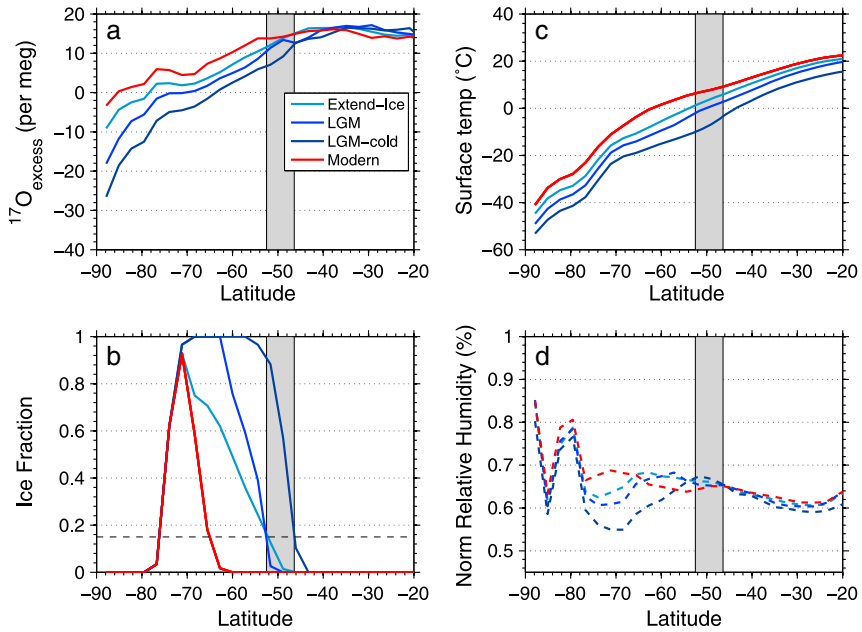

Figure 11. Modern, Extend-Ice, LGM, and LGM-cold GCM simulations for West Antarctica (70°W to 170°W) annual average using high supersaturation ($S = 1 - 0.007\,T$). (a) $^{17}O_{excess}$ versus latitude, gray band marks the range of latitude of maximum sea ice extent using a minimum threshold of 0.15 ice fraction. (b) Ice fraction for all simulations versus latitude. (c) Surface temp versus latitude for all three simulations. (d) Normalized relative humidity (rh_n %) versus latitude. Note that the few percent (2–3%) change in rh_n over the midlatitude is insufficient to explain the magnitude of $^{17}O_{excess}$ changes based on ~ −1 per meg/% rh_n from *Risi et al.* [2010a].

sites in East Antarctica, which tend to receive greater moisture from mid- to high-latitude source regions with greater rh_n, elevated $^{17}O_{excess}$ values are observed, opposite to that expected if rh_n were the determining factor.

It has been argued that observed glacial to interglacial $^{17}O_{excess}$ differences between ice core locations is due to different oceanic moisture source regions, controlled by their respective surface humidity [*Landais et al.*, 2008; *Risi et al.*, 2010a; *Winkler et al.*, 2012]. Yet our simulations show that fractionation under supersaturated conditions alone is sufficient to account for the magnitude of glacial-interglacial change, provided a relatively strong sensitivity of supersaturation to temperature. In the same simulations, rh_n increases only a few percent over the Southern Ocean moisture source regions (20 to 55°S), too little to account for the simulated $^{17}O_{excess}$ changes, the magnitude of which is clearly determined by the degree of fractionation in transport. Larger changes (~10%) in rh_n do occur over the sea ice region but are of the wrong sign (i.e., $^{17}O_{excess}$ on the continent decreases when rh_n decreases). In any case, moisture fluxes from the sea ice region are small and do not contribute a significant fraction of moisture to the continent.

The simple parameterization of supersaturation in terms of temperature does not fully capture all the ice core observations. Indeed, depending on the supersaturation sensitivity, the modeled LGM versus present-day $^{17}O_{excess}$ change may be underestimated in some locations and overestimated in others. Comparison of the different model experiments suggests that prescribed sea ice boundary conditions play an important role. Referring to the gray bars in Figures 11 and 12, which illustrate the maximum latitude of sea ice extent, we note that there is a marked change in the latitudinal gradient in $^{17}O_{excess}$ that occurs approximately at the latitude of the sea ice margin. In each of the LGM, LGM-cold, and Extend-Ice experiments, compared with the Modern experiment, there is correspondence between the location of the maximum sea ice extent and change in slope of the $^{17}O_{excess}$ gradient.

Although it is difficult to separate the influence of sea ice from the influence of temperature (because the two are highly correlated), the change in $^{17}O_{excess}$ between each progressively colder model experiment does not

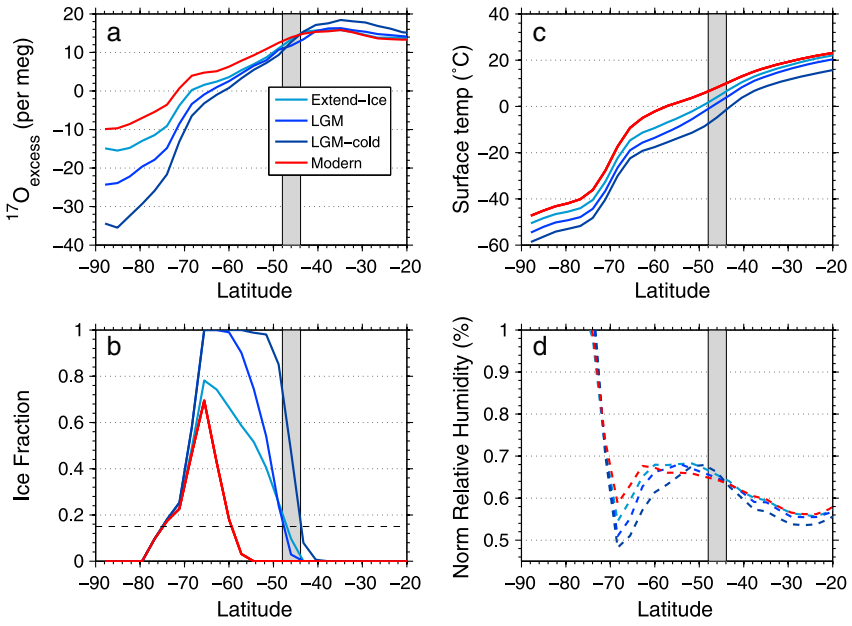

Figure 12. Modern, Extend-Ice, LGM, and LGM-cold GCM simulations for East Antarctica (290°E to 160°E) annual average using high supersaturation ($S = 1 - 0.007\,T$). (a) $^{17}O_{excess}$ for all simulations versus latitude, gray band same as in Figure 11. (b) Ice fraction versus latitude. (c) Surface temperature versus latitude. (d) Normalized relative humidity (rh_n %) versus latitude.

scale directly with the lower temperatures. Rather, the $^{17}O_{excess}$ gradient steepens for the same respective change in temperature in each model experiment. For example, in the Modern simulation the zonal average slope in $^{17}O_{excess}$ is −0.53 per meg/°C for temperatures between −20°C and − 45°C; this increases in magnitude to −0.63, −0.70, and −0.87 per meg/°C for Extend-Ice, LGM, and LGM-cold, respectively (Figure S3). Note that the increasing $^{17}O_{excess}$/temperature gradient also tracks the pattern of greater sea ice fraction for each colder model simulation. Furthermore, in the Extend-Ice simulation, the strongest response in $^{17}O_{excess}$ occurs during austral fall and winter, the periods of greatest sea ice expansion and maximum ice extent, while there is no change in $^{17}O_{excess}$ during austral summer (JFM), despite cooler temperatures relative to the Modern simulation.

These results suggest that $^{17}O_{excess}$ is sensitive to sea ice boundary conditions. The expansion of sea ice in these experiments influences $^{17}O_{excess}$ in at least two ways. First, expanded sea ice cover increases the meridional temperature gradient, with the result that poleward traveling air masses reach cold conditions sooner, resulting in stronger supersaturation and greater kinetic fractionation; this effect largely explains the change in slope of $^{17}O_{excess}$ approximately at the sea ice margin. Second, greater sea ice cover reduces the availability of local (high-latitude) moisture recharge of relatively enriched $^{17}O_{excess}$ water vapor into the atmosphere. In our model setup, sea ice concentration is binary (grids are either "on" or "off") and may not produce realistic estimates of sea ice concentration change, which would influence the degree to which the moisture-recharge effect is important. In general, though, both of these influences tend to lower $^{17}O_{excess}$ over the Antarctic continent. As the process of isotope fractionation acts as an integrator of the entire moisture transport path, changes in both ice fraction and extent would be expected to have a cumulative impact on the $^{17}O_{excess}$ in precipitation.

4.2. Interpretation of Individual Antarctic $^{17}O_{excess}$ Records

We conclude that the sign and magnitude of LGM to EH $^{17}O_{excess}$ changes apparent in the ice core time series can be explained by a common process: strong sensitivity of supersaturation to temperature during kinetic fractionation. One important implication of this result is that it is unnecessary to invoke the contribution of stratospheric moisture as an explanation for the Vostok $^{17}O_{excess}$ record. *Miller* [2008] suggested that, due to the low annual accumulation and high elevation of the East Antarctic plateau, the large glacial-interglacial $^{17}O_{excess}$ change at Vostok could reflect input from high-$^{17}O_{excess}$ water vapor with a

stratospheric source. Yet the LGM to Early Holocene change in $^{17}O_{excess}$ at WAIS Divide is similar to that at Vostok. Based on present-day downward fluxes [*Stohl and Sodemann*, 2010; *Winkler et al.*, 2013], stratospheric water vapor contributes ~10^{-5} of the 22 cm a^{-1} annual mean ice accumulation rate at WAIS Divide, an order of magnitude less than the 0.014% calculated for Vostok by *Winkler et al.* [2013]. Even if the contribution of stratospheric input were 10 times greater for WAIS Divide, assuming a stratospheric $^{17}O_{excess}$ signature of ~3000 per meg [*Zahn et al.*, 2006; *Winkler et al.*, 2013], it would change the $^{17}O_{excess}$ by less than 0.12 per meg.

Our model results additionally show that sea ice extent plays an important role in determining the magnitude of $^{17}O_{excess}$ changes on glacial-interglacial timescales. In general, greater sea ice extent amplifies the $^{17}O_{excess}$ response to temperature. In this context, differences among the different ice core sites that are not fully captured by the model results discussed above are informative.

Taylor Dome and Talos Dome share similar elevations (~2300 m) and mean annual temperature (~40°C) and are in close proximity to one another. These sites are often referred to as "coastal," since they are both within less than 300 km from periodically open water. However, their moisture sources are quite different. Back trajectory modeling shows that Taylor Dome receives more than 60% of its total precipitation from the Pacific, along a trajectory that crosses over West Antarctica [*Scarchilli et al.*, 2010]; thus, the majority of the trajectories cross over the ice sheet. Talos Dome receives nearly twice the accumulation of Taylor Dome and about half of its total precipitation originates from the Indian Ocean; about one third originates from the Ross Sea [*Scarchilli et al.*, 2010].

At Talos Dome, the model versus data discrepancy is relatively large: the ice core observations show no change between the LGM and EH, while the model, using $b = 0.007$ which best fits most other locations, including Taylor Dome, simulates a change of ~12 per meg for LGM boundary conditions. Based on the similar LGM-EH $\delta^{18}O$ change (~5.5‰) at both Taylor Dome and Talos Dome, we can assume that the temperature changes were comparable; temperature-driven changes in supersaturation effects on $^{17}O_{excess}$ should also have been similar. This implies that either the air mass trajectory changes affected Talos Dome and Taylor Dome differently or that regional boundary conditions were different or both. Note that Talos Dome is situated upwind of Terra Nova Bay and the Ross Sea Polynya in the western Ross Sea. In winter, the Ross Sea Polynya contributes significantly to mesocyclonic activity, which favors the advection of moist maritime air into the interior. Local changes to features like this—which are not captured in the relatively coarse grid of our GCM simulations—could explain differences between these sites. For example, expansion of the Ross Sea ice shelf to form the Ross Sea Ice Sheet during the LGM [e.g., *Hall et al.*, 2000]; expanded sea ice north of the ice sheet margin would have cut off local moisture sources and would perhaps have had a larger impact on the isotopic composition of precipitation at Talos Dome than Taylor Dome.

The importance of local boundary conditions is also illustrated by comparing the model results for both Taylor Dome and Talos Dome with those for Siple Dome. The LGM model simulation ($b = 0.007$) produces a ~12 per meg decrease in $^{17}O_{excess}$ at Taylor Dome and Talos Dome, relative to present-day, but little to no change at Siple Dome. In the LGM simulation there is a significant increase in sea ice in the western Ross Sea but no change in the eastern Ross Sea (adjacent to Siple Dome). In the model simulations, local moisture sources near Siple Dome change little; since this low elevation (600 m), truly coastal site is relatively warm and not subject to significant supersaturation effects, and since rh_n does not change significantly between the two simulations, there is no resulting change of $^{17}O_{excess}$. This is consistent with the suggestion of *Winkler et al.* [2012] that warmer, more coastal sites should be less influenced by the effects of supersaturation and therefore more faithfully record changes of rh_n (or in this case, lack thereof), than more interior sites. In the actual ice core measurements, there is no evidence of a glacial-interglacial change in $^{17}O_{excess}$ at Siple Dome, supporting this understanding. Nevertheless, these comparisons also suggest that using $^{17}O_{excess}$ from coastal sites to infer moisture source changes is likely to be problematic. In general, such sites are more likely to be influenced by local peculiarities in ocean surface conditions than more interior sites, and therefore, despite the reduced sensitivity to supersaturation, coastal cores may not provide representative information. When interpreting $^{17}O_{excess}$ data in detail as additional higher-resolution records are obtained, it will be important to consider regional details such as air mass trajectories and sea ice concentration.

Finally, some unique features of the WAIS Divide ice core record are noted. As discussed in *WAIS Divide Project Members* [2013], the WDC $\delta^{18}O$ record shows an early deglacial warming, beginning between 22 and 20 ka.

East Antarctic ice core $\delta^{18}O$ records show little change until a relatively abrupt $\delta^{18}O$ increase at ~18 ka. Model experiments using a symmetric sea ice reduction suggest that the earlier warming at WAIS Divide could reflect the greater sensitivity of this site to sea ice change [*WAIS Divide Project Members*, 2013]. Consistent with this, the WDC $^{17}O_{excess}$ record shows an inflection point occurring at ~22 ka, while $^{17}O_{excess}$ at both Vostok and Dome C begins to increase between ~ 18.5 ka and 17.5 ka. Based on the model experiments discussed above, we propose that the early increase in $^{17}O_{excess}$ at ~22 ka in WDC results from early decreasing sea ice extent resulting in a reduced influence of kinetic fractionation on $^{17}O_{excess}$, owing both to warmer temperatures, greater local moisture recharge, and less transit distance over sea ice. The difference between LGM and LGM-cold model experiments show that the response of sea ice can be asymmetric. Expressions of early deglacial changes in SST and sea ice extent have been identified in other high-latitude Southern Hemisphere records and are suggestive of greater changes in the Pacific sector than elsewhere [*Kanfoush*, 2000; *Lamy et al.*, 2007; *Collins et al.*, 2012], which would contribute to the different timing signature observed in $^{17}O_{excess}$ between East and West Antarctica.

Another notable feature of the WDC $^{17}O_{excess}$ record is the unambiguous rise in $^{17}O_{excess}$ beginning at ~15 ka. WDC $^{17}O_{excess}$ increases by ~10 per meg over the ~400 year period prior to the Antarctic Isotope Maximum (AIM) 1 peak in $\delta^{18}O$, which in turn is near-coincident with the rapid increase in $\delta^{18}O$ in Greenland ice cores and the abrupt rise in methane at ~14.7 ka B.P. that defines the beginning of the Bølling-Allerød warm interval [*WAIS Divide Project Members*, 2013]. Relative to the background variability in $^{17}O_{excess}$, the magnitude of the $^{17}O_{excess}$ rise is much larger than seen in the d_{ln} (or d_{excess}) record in WDC, suggesting a significant change in boundary conditions. We speculate that this reflects a decrease in sea ice concentration preceding the isotope maximum, as indicated for example by ocean model simulations of AIM events [*Knorr and Lohmann*, 2003]. We note that there is a small but significant decrease in the ssNa concentration during this interval, also consistent with decreasing sea ice [*Wolff et al.*, 2006; *WAIS Divide Project Members*, 2013].

During the Holocene (12 to 0 ka) interval, $^{17}O_{excess}$ in WDC varies little compared to the magnitude of glacial-interglacial change. However, it exhibits a long-term negative trend beginning at ~9 ka. We note that a similar long-term decrease has been observed in other Southern Hemisphere and SST proxy records [*Lamy et al.*, 2002; *Nielsen et al.*, 2004; *Lamy et al.*, 2007], which has been suggested to result from decreasing austral spring orbital forcing and increasing sea ice extent and/or concentration [*Steig et al.*, 1998a; *Hodell et al.*, 2001; *Renssen et al.*, 2005]. This is again consistent with our finding that sea ice exerts a significant control on $^{17}O_{excess}$.

4.3. Implications for Modeling $^{17}O_{excess}$

The development of $^{17}O_{excess}$ ice core records covering the last glacial-to-interglacial transition, in combination with d_{ln}, provides an important new constraint for water isotope-enabled GCM simulations. The amount of kinetic fractionation in the model, parameterized by a temperature-dependent supersaturation function, has a strong influence on the magnitude and sign of the $^{17}O_{excess}$ spatial gradient. As we have shown, capturing the spatial pattern of glacial-interglacial change in $^{17}O_{excess}$ using the standard linear parameterization of supersaturation requires greater kinetic fractionation during ice formation than has typically been used in the literature [*Hoffmann et al.*, 1998; *Werner and Heimann*, 2002; *Schmidt et al.*, 2005; *Masson-Delmotte et al.*, 2008; *Werner et al.*, 2011]. However, the linear parameterization for supersaturation as a simple function of temperature, as used in most work (including that presented here) was developed over 35 years ago, and the choice of a linear dependence on temperature is somewhat arbitrary. Indeed, *Jouzel and Merlivat* [1984] also proposed exponential and power law dependencies. The increasing availability of $^{17}O_{excess}$ data should inspire reevaluation of the treatment of supersaturation in GCMs. The routine inclusion of $^{17}O_{excess}$ within GCMs also has the potential to help improve other aspects of the model hydrological cycle beyond those related to ice core research, such as the partitioning of water vapor versus ice in clouds, rain reevaporation during convective downdrafts, and surface evaporative processes [*Risi et al.*, 2008; *Landais et al.*, 2010; *Risi et al.*, 2010b].

As already noted, all of our model simulations underestimate the mean $^{17}O_{excess}$ over Antarctica. This may largely reflect uncertainty in the mean seawater $^{17}O_{excess}$ value but may also reflect biases in the model climatology. In particular, the relatively low model resolution means that the steepness of the Antarctic

continental margin is underestimated, which may allow greater penetration of marine air mass intrusion into Antarctica, making the Antarctic interior more influenced by marine sources than it actually is [*Noone and Simmonds*, 2004; *Ding et al.*, 2011]. Indeed, we find that the modeled annual precipitation at WAIS Divide is ~50 % higher than observed. Analysis of different model resolutions in ECHAM5 by *Werner et al.* [2011] showed that, in general, higher-resolution simulations produced better agreement with observational data sets. In particular, the relationship between d_{excess} and δD is in much better agreement with the *Masson-Delmotte et al.* [2008] Antarctic isotope database in the ECHAM5 T159 simulation.

Although the ECHAM4.6 model qualitatively reproduces both the present-day spatial gradient and the magnitude of LGM-EH change in $^{17}O_{excess}$, inconsistencies between the ice core observations and model experiments highlight the additional work needed. We identify a number of important factors relevant to accurately simulating $^{17}O_{excess}$, d_{ln}, and d_{excess}.

First, additional measurements of $\delta^{18}O$, d_{excess}, and $^{17}O_{excess}$ in laboratory experiments at subzero temperatures are needed to refine the relationship of temperature-dependent equilibrium fractionation between all isotope species, which can provide a more solid foundation from which to investigate kinetic fractionation effects on d_{excess} (and d_{ln}). The benchmark for isotope-enabled GCM validation in polar regions has been the reproduction of the observed d_{excess} spatial gradient, in conjunction with the highly depleted δD or $\delta^{18}O$ values. There has been difficulty simulating realistic values of d_{excess} in the East Antarctic interior, which typically have too steep a spatial gradient in the simulations. In ECHAM4.6, the inclusion of a temperature-dependent diffusion fractionation factor for δD [*Luz et al.*, 2009], as well the most up-to-date equilibrium fractionation factors for δD and $\delta^{18}O$ below freezing [*Ellehøj et al.*, 2013] have reduced the steep spatial gradient, in better agreement with d_{excess} observations.

Second, a key goal should be to improve the relatively simple kinetic fractionation parameterizations used in both simple 1-D isotope models and intermediate complexity isotope models, as well as in most GCMs. In particular, the increased computational capacity available for GCMs permits moving beyond the fairly simple supersaturation parameterization to explicitly determine supersaturation, dependent on detailed cloud microphysics (e.g., types of condensation nuclei). The subgrid scale at which phase changes occur require kinetic fractionation to still be parameterized; however, more advanced parameterizations of kinetic fractionation are being implemented that better account for convective cloud processes in the tropical regions [*Risi et al.*, 2008; *Blossey et al.*, 2010; *Landais et al.*, 2010]. Similarly, more sophisticated parameterizations that incorporate surface kinetic fractionation effects due to differences in water droplet size, ice crystal morphology (e.g., columnar versus dendritic) are needed. These surface kinetic fractionation effects may vary greatly between regions where dry deposition of tiny ice crystals (diamond dust) prevail, like the East Antarctic plateau, compared to wet deposition sites in coastal regions [*Nelson*, 2011]. The sensitivity of $^{17}O_{excess}$ to kinetic fractionation makes it an ideal indicator for testing such aspects of the model physics.

The importance of supersaturation in determining the behavior of $^{17}O_{excess}$ and d_{ln} (or d_{excess}) also suggests that further work must be done to characterize the kinetic fractionation effects during ice crystal formation on a microscopic level, both with additional empirical lab studies and in situ low temperature/high altitude measurements. The early study by *Jouzel and Merlivat* [1984] on kinetic isotope fractionation during snow formation was performed on the frost grown onto a cooling plate (−20°C) from room temperature (20°C) without conditions that controlled the supersaturation ratio, resulting in an overestimated supersaturation ration of 2.00 [*Uemura et al.*, 2005]. Recent work by *Uemura et al.* [2005] produced experimental conditions that mimicked those of mixed clouds in which both vapor and supercooled water droplets coexist due to the realistic temperature range (−12 to −15°C). Their results produced lower supersaturation ratios than *Jouzel and Merlivat* [1984], but the range of supersaturation ratios (S = 1.165 to 1.221) at −15°C are consistent with a higher sensitivity of supersaturation where $b > 0.007$. Measurements performed at colder temperatures ranging from −20 to −50°C would be invaluable.

Finally, to improve the interpretation of Antarctic $^{17}O_{excess}$, more measurements on surface snow and ice cores from both coastal and interior sites are needed. Acquiring additional $^{17}O_{excess}$ measurements on transects that span coastal to interior sites, like those obtained by *Landais et al.* [2008], would provide higher spatial resolution, important for examining the sensitivity of $^{17}O_{excess}$ to regional details such as coastal moisture sources (e.g., leads and polynyas) and orographic features.

5. Conclusions

Our ice core measurements, in combination with those from *Landais et al.* [2008] and *Winkler et al.* [2012] show that there is a strong spatial gradient of $^{17}O_{excess}$ across Antarctica, with elevated values in the coastal and marine-influenced regions and lower values in the central East Antarctic plateau. The modern spatial gradient in $^{17}O_{excess}$ is best captured with a strong sensitivity of supersaturation to temperature. The data also show that there are large changes in the inland regions of both East and West Antarctica, but little change in the coastal regions over the last deglaciation (LGM to Early Holocene). An atmospheric GCM forced with LGM boundary conditions, and the same strong sensitivity of supersaturation to temperature that best matches the modern data, reproduces the observed sign, magnitude, and spatial pattern of LGM to Early Holocene change in $^{17}O_{excess}$. We conclude that kinetic isotope effects result from supersaturation of water vapor over ice dominate the spatial pattern of modern $^{17}O_{excess}$ in Antarctic precipitation as well as the pattern of change through the last deglaciation. These results imply a limited role of changes in relative humidity in determining the glacial-interglacial $^{17}O_{excess}$ in Antarctic precipitation and show that the influence of stratospheric water vapor inputs is probably negligible.

In the GCM experiments, there is correspondence between the latitude of maximum sea ice extent and a change in $^{17}O_{excess}$ gradient, indicating that the sea ice boundary conditions play a role in controlling $^{17}O_{excess}$. A principal control on the amount of kinetic fractionation is the temperature gradient between moisture source and precipitation site, and in our GCM experiments, an effective way to increase the temperature gradient is by expansion of sea ice. The expansion of sea ice causes poleward traveling moisture to encounter colder conditions earlier, resulting in the onset of supersaturation conditions, and initiating a decrease in $^{17}O_{excess}$. A secondary result of sea ice cover is the reduction of evaporative moisture recharge to the overlying air mass, which limits the addition of relatively enriched $^{17}O_{excess}$ water vapor from the high-latitude ocean surface.

Most previous studies have relied on changes in normalized relative humidity at the moisture origin to explain the observed glacial-interglacial changes in $^{17}O_{excess}$. Despite the ~10° northward expansion of sea ice in both the LGM and present-day Extend-Ice experiments, we simulate only minor changes in the relative humidity at the ocean surface. Furthermore, $^{17}O_{excess}$ over Antarctica does not respond as would be expected if surface relative humidity were the main driver. Sea ice changes and the associated temperature changes alone—with no significant change in moisture source humidity—are sufficient to explain the observed $^{17}O_{excess}$ glacial-interglacial changes at most locations in Antarctica where observations exist.

Due to the few $^{17}O_{excess}$ ice core measurements and inconsistently normalized data, interpretation of $^{17}O_{excess}$ in Antarctic ice cores has been challenging. The measurements from the WDC record provide the first complete $^{17}O_{excess}$ record through the LGM to the present-day, indicating an early deglacial change in $^{17}O_{excess}$ around 22 ka, an early Holocene optimum from 11.5 to 9.5 ka, and a post EH optimum period of $^{17}O_{excess}$ decline. We propose that expansion of sea ice during the LGM and post EH optimum led to the lowering of $^{17}O_{excess}$ during these periods. The response of $^{17}O_{excess}$ at 22 ka, which predates changes in both $^{17}O_{excess}$ and $\delta^{18}O$ in Dome C and Vostok by approximately 4000 years, suggests an early retreat of sea ice in the southern Pacific Ocean, and supports the findings of *WAIS Divide Project Members* [2013] that changes in sea ice extent may explain the early $\delta^{18}O$ increases in WDC at 22 and 20 ka.

Even with strong supersaturation sensitivity and expanded sea ice boundary conditions, we find that our GCM simulations generally underestimate the magnitude of LGM-EH change in $^{17}O_{excess}$ in the WDC record. We speculate that reflects a combination of modeled modern temperatures and modeled LGM temperatures that are too warm; the "LGM-cold" experiment with temperature reduced an additional 4°C supports this view. Preliminary estimates of the glacial-interglacial temperature change at WAIS Divide from borehole temperature reconstructions indicate a larger temperature change than simulated in our experiments (K. Cuffey, personal communication, 2013). This suggests that $^{17}O_{excess}$ could provide an independent constraint on the magnitude of glacial-interglacial temperature change. However, site-specific differences between the observed and modeled ice core $^{17}O_{excess}$ data suggest that the climate interpretation of $^{17}O_{excess}$ at particular locations will require assessment of regional circulation patterns, sea ice concentration, and local meteorological conditions.

Acknowledgments
This work was supported by National Science Foundation (NSF) OPP grants 0837990 and 1043092 to E.J.S. We thank K. Samek, B. Vanden Heuvel, and R. Teel for their assistance with the isotope measurements. We also thank J. Pedro for discussions, J. Schmitt for use of the Monte Carlo Averaging code, B. Stenni for providing the unpublished Talos Dome $\delta^{18}O$ and δD data, and D. Roche for figure permissions. The authors appreciate the support of the WAIS Divide Science Coordination Office (K. Taylor, M. Twickler, and J. Souney) for the collection and distribution of the WAIS Divide ice core; Ice Drilling and Design and Operations for drilling; and the National Ice Core Laboratory for curating the core. Many thanks to two anonymous reviewers for valuable comments and suggestions. Data from this paper are available from the National Snow and Ice Data Center (www.nsidc.org).

References

Abe, O. (2008), Isotope fractionation of molecular oxygen during adsorption/desorption by molecular sieve zeolite, *Rapid Commun. Mass Spectrom.*, *22*(16), 2510–2514.

Baker, L., I. Franchi, J. Maynard, I. Wright, and C. Pillinger (2002), A technique for the determination of $^{18}O/^{16}O$ and $^{17}O/^{16}O$ isotopic ratios in water from small liquid and solid samples, *Anal. Chem.*, *74*(7), 1665–1673.

Barkan, E., and B. Luz (2005), High precision measurements of $^{17}O/^{16}O$ and $^{18}O/^{16}O$ ratios in H_2O, *Rapid Commun. Mass Spectrom.*, *19*(24), 3737–3742.

Barkan, E., and B. Luz (2007), Diffusivity fractionations of $H_2{}^{16}O/H_2{}^{17}O$ and $H_2{}^{16}O/H_2{}^{18}O$ in air and their implications for isotope hydrology, *Rapid Commun. Mass Spectrom.*, *21*, 2999–3005.

Berger, A. (1978), Long-term variations of caloric insolation resulting from the Earth's orbital elements, *Quatern. Res.*, *9*(2), 139–167, doi:10.1016/0033-5894(78)90064-9.

Blossey, P. N., Z. Kuang, and D. M. Romps (2010), Isotopic composition of water in the tropical tropopause layer in cloud-resolving simulations of an idealized tropical circulation, *J. Geophys. Res.*, *115*, D24309, doi:10.1029/2010JD014554.

Braconnot, P., B. Otto-Bliesner, S. Harrison, S. Joussaume, J. Y. Peterchmitt, A. Abe-Ouchi, M. Crucifix, E. Driesschaert, T. Fichefet, and C. D. Hewitt (2007), Results of PMIP2 coupled simulations of the mid-Holocene and Last Glacial Maximum–Part 1: Experiments and large-scale features, *Clim. Past*, *3*(2), 261–277.

Brook, E. J., J. W. C. White, A. S. M. Schilla, M. L. Bender, B. Barnett, J. P. Severinghaus, K. C. Taylor, R. B. Alley, and E. J. Steig (2005), Timing of millennial-scale climate change at Siple Dome, West Antarctica, during the last glacial period, *Quaternary Sci. Rev.*, *24*(12-13), 1333–1343, doi:10.1016/j.quascirev.2005.02.002.

Collins, L. G., J. Pike, C. S. Allen, and D. A. Hodgson (2012), High-resolution reconstruction of southwest Atlantic sea-ice and its role in the carbon cycle during marine isotope stages 3 and 2, *Paleoceanography*, *27*, PA3217, doi:10.1029/2011PA002264.

Dansgaard, W. (1964), Stable isotopes in precipitation, *Tellus*, *16*, 436–468.

Ding, Q., E. J. Steig, D. S. Battisti, and M. Küttel (2011), Winter warming in West Antarctica caused by central tropical Pacific warming, *Nat. Geosci.*, *4*(6), 398–403, doi:10.1038/ngeo1129.

Ellehøj, M. D., H. C. Steen-Larsen, S. J. Johnsen, and M. B. Madsen (2013), Ice-vapor equilibrium fractionation factor of hydrogen and oxygen isotopes: Experimental investigations and implications for stable water isotope studies, *Rapid Commun. Mass Spectrom.*, *27*(19), 2149–2158, doi:10.1002/rcm.6668.

EPICA Community Members (2004), Eight glacial cycles from an Antarctic ice core, *Nature*, *429*(6992), 623–628, doi:10.1038/nature02599.

EPICA Community Members (2006), One-to-one coupling of glacial climate variability in Greenland and Antarctica, *Nature*, *444*(7116), 195–198, doi:10.1038/nature05301.

Frezzotti, M., G. Bitelli, and P. de Michelis (2004), Geophysical survey at Talos Dome, East Antarctica: The search for a new deep-drilling site, *Ann. Glaciol.*, *39*(1), 423–432.

Fujita, K., and O. Abe (2006), Stable isotopes in daily precipitation at Dome Fuji, East Antarctica, *Geophys. Res. Lett.*, *33*, L18503, doi:10.1029/2006GL026936.

Gat, J. (1996), Oxygen and hydrogen isotopes in the hydrologic cycle, *Annu. Rev. Earth Planet. Sci.*, *24*, 225–262.

Gersonde, R., X. Crosta, A. Abelmann, and L. Armand (2005), Sea-surface temperature and sea ice distribution of the Southern Ocean at the EPILOG Last Glacial Maximum—A circum-Antarctic view based on siliceous microfossil records, *Quaternary Sci. Rev.*, *24*(7–9), 869–896, doi:10.1016/j.quascirev.2004.07.015.

Hall, B. L., G. H. Denton, and C. H. Hendy (2000), Evidence from Taylor Valley for a grounded ice sheet in the Ross Sea, Antarctica, *Geogr. Ann. A.*, *82*(2–3), 275–303.

Helsen, M. M., R. S. W. van de Wal, and M. R. van den Broeke (2007), The isotopic composition of present-day Antarctic snow in a Lagrangian atmospheric simulation*, *J. Clim.*, *20*(4), 739–756, doi:10.1175/JCLI4027.1.

Hodell, D. A., S. L. Kanfoush, A. Shemesh, X. Crosta, C. D. Charles, and T. P. Guilderson (2001), Abrupt cooling of Antarctic surface waters and sea ice expansion in the south Atlantic sector of the southern ocean at 5000 cal yr B.P, *Quatern. Res.*, *56*(2), 191–198, doi:10.1006/qres.2001.2252.

Hoffmann, G., M. Werner, and M. Heimann (1998), Water isotope module of the ECHAM atmospheric general circulation model: A study on timescales from days to several years, *J. Geophys. Res.*, *103*(D14), 16,871–16,896, doi:10.1029/98JD00423.

Hoffmann, G., M. Cuntz, J. Jouzel, and M. Werner (2005), A systematic comparison between the IAEA/GNIP isotope network and the ECHAM 4 atmospheric general circulation model, in *Isotopes in the Water Cycle: Past, Present and Future of a Developing Science*, pp. 303–320, Springer, Netherlands.

Jouzel, J., and L. Merlivat (1984), Deuterium and oxygen 18 in precipitation: Modeling of the isotopic effects during snow formation, *J. Geophys. Res.*, *89*, 11,749–11,757, doi:10.1029/JD089iD07p11749.

Jouzel, J., F. Vimeux, N. Caillon, G. Delaygue, G. Hoffmann, V. Masson-Delmotte, and F. Parrenin (2003), Magnitude of isotope/temperature scaling for interpretation of central Antarctic ice cores, *J. Geophys. Res.*, *108*(D12), 4361, doi:10.1029/2002JD002677.

Jouzel, J., et al. (2007), Orbital and millennial antarctic climate variability over the past 800,000 years, *Science*, *317*(5839), 793–796, doi:10.1126/science.1141038.

Kanfoush, S. L. (2000), Millennial-scale instability of the antarctic Ice sheet during the Last Glaciation, *Science*, *288*(5472), 1815–1819, doi:10.1126/science.288.5472.1815.

Kavanaugh, J. L., and K. M. Cuffey (2003), Space and time variation of $\delta^{18}O$ and δD in Antarctic precipitation revisited, *Global Biogeochem. Cycles*, *17*(1), 1017, doi:10.1029/2002GB001910.

Knorr, G., and G. Lohmann (2003), Southern Ocean origin for the resumption of Atlantic thermohaline circulation during deglaciation, *Nature*, *424*(6948), 532–536, doi:10.1038/nature01855.

Lamy, F., C. Rühlemann, D. Hebbeln, and G. Wefer (2002), High- and low-latitude climate control on the position of the southern Peru-Chile Current during the Holocene, *Paleoceanography*, *17*(2), 1028, doi:10.1029/2001PA000727.

Lamy, F., J. Kaiser, H. W. Arz, D. Hebbeln, U. Ninnemann, O. Timm, A. Timmermann, and J. R. Toggweiler (2007), Modulation of the bipolar seesaw in the Southeast Pacific during Termination 1, *Earth Planet. Sci. Lett.*, *259*(3-4), 400–413, doi:10.1016/j.epsl.2007.04.040.

Landais, A., E. Barkan, and B. Luz (2008), Record of $\delta^{18}O$ and ^{17}O-excess in ice from Vostok Antarctica during the last 150,000 years, *Geophys. Res. Lett.*, *35*, L02709, doi:10.1029/2007GL032096.

Landais, A., C. Risi, S. Bony, F. Vimeux, L. Descroix, S. Falourd, and A. Bouygues (2010), Combined measurements of ^{17}O-excess and d-excess in African monsoon precipitation: Implications for evaluating convective parameterizations, *Earth Planet. Sci. Lett.*, *298*(1), 104–112.

Landais, A., A. Ekaykin, E. Barkan, R. Winkler, and B. Luz (2012a), Seasonal variations of ^{17}O-excess and d-excess in snow precipitation at Vostok station, East Antarctica, *J. Glaciol.*, *58*(210), 725–733, doi:10.3189/2012JoG11J237.

Landais, A., H. C. Steen-Larsen, M. Guillevic, V. Masson-Delmotte, B. Vinther, and R. Winkler (2012b), Triple isotopic composition of oxygen in surface snow and water vapor at NEEM (Greenland), *Geochim. Cosmochim. Acta*, *77*, 304–316, doi:10.1016/j.gca.2011.11.022.

Legrand, M., and R. J. Delmas (1985), Spatial and temporal variations of snow chemistry in Terre Adelie (East Antarctica), *Ann. Glaciol.*, *7*, 20–25.

Luz, B., and E. Barkan (2010), Variations of $^{17}O/^{16}O$ and $^{18}O/^{16}O$ in meteoric waters, *Geochim. Cosmochim. Acta*, *74*(22), 6276–6286, doi:10.1016/j.gca.2010.08.016.

Luz, B., E. Barkan, R. Yam, and A. Shemesh (2009), Fractionation of oxygen and hydrogen isotopes in evaporating water, *Geochim. Cosmochim. Acta*, *73*(22), 6697–6703.

Majoube, M. (1971), Oxygen-18 and deuterium fractionation between water and steam, *J. Chim. Phys. Phys. Chim. Biol.*, *68*(10), 1423–1436.

Masson-Delmotte, V., et al. (2008), A review of Antarctic surface snow isotopic composition: Observations, atmospheric circulation, and isotopic modeling, *J. Clim.*, *21*(13), 3359–3387, doi:10.1175/2007JCLI2139.1.

Matsuhisa, Y., J. R. Goldsmith, and R. N. Clayton (1978), Mechanisms of hydrothermal crystallization of quartz at 250°C and 15 kbar, *Geochim. Cosmochim. Acta*, *42*(2), 173–182, doi:10.1016/0016-7037(78)90130-8.

Merlivat, L., and J. Jouzel (1979), Global climatic interpretation of the deuterium-oxygen 18 relationship for precipitation, *J. Geophys. Res.*, *84*(C8), 5029–5033, doi:10.1029/JC084iC08p05029.

Miller, M. F. (2008), Comment on "Record of $\delta^{18}O$ and ^{17}O-excess in ice from Vostok Antarctica during the last 150,000 years" by Amaelle Landais et al, *Geophys. Res. Lett.*, *35*, L23708, doi:10.1029/2008GL034505.

Motoyama, H., N. Hirasawa, K. Satow, and O. Watanabe (2005), Seasonal variations in oxygen isotope ratios of daily collected precipitation and wind drift samples and in the final snow cover at Dome Fuji Station, Antarctica, *J. Geophys. Res.*, *110*, D11106, doi:10.1029/2004JD004953.

Nelson, J. (2011), Theory of isotopic fractionation on facetted ice crystals, *Atmos. Chem. Phys.*, *11*(22), 11,351–11,360, doi:10.5194/acp-11-11351-2011.

Nielsen, S. H. H., N. Koç, and X. Crosta (2004), Holocene climate in the Atlantic sector of the Southern Ocean: Controlled by insolation or oceanic circulation?, *Geology*, *32*(4), 317, doi:10.1130/G20334.1.

Noone, D., and I. Simmonds (2004), Sea ice control of water isotope transport to Antarctica and implications for ice core interpretation, *J. Geophys. Res.*, *109*, D07105, doi:10.1029/2003JD004228.

Orsi, A. J., B. D. Cornuelle, and J. P. Severinghaus (2012), Little Ice Age cold interval in West Antarctica: Evidence from borehole temperature at the West Antarctic Ice Sheet (WAIS) Divide, *Geophys. Res. Lett.*, *39*, L09710, doi:10.1029/2012GL051260.

Otto-Bliesner, B. L., E. C. Brady, G. Clauzet, R. Tomas, S. Levis, and Z. Kothavala (2006), Last glacial maximum and Holocene climate in CCSM3, *J. Clim.*, *19*(11), 2526–2544, doi:10.1175/JCLI3748.1.

Peltier, W. R. (2004), Global glacial isostasy and the surface of the ice-age Earth: The ICE-5G (VM2) model and GRACE, *Annu. Rev. Earth Planet. Sci.*, *32*, 111–149, doi:10.1146/annurev.earth.32.082503.144359.

Petit, J. R., J. White, N. W. Young, J. Jouzel, and Y. S. Korotkevich (1991), Deuterium excess in recent Antarctic Snow, *J. Geophys. Res.*, *96*(D3), 5113–5122, doi:10.1029/90JD02232.

Petit, J. R., et al. (1999), Climate and atmospheric history of the past 420,000 years from the Vostok ice core, Antarctica, *Nature*, *399*(6735), 429–436, doi:10.1038/20859.

Radok, U., and R. C. Lile (1977), A year of snow accumulation at Plateau Station, *Antarct. Res.*, *25*, 17–26.

Renssen, H., H. Goosse, T. Fichefet, V. Masson-Delmotte, and N. Koç (2005), Holocene climate evolution in the high-latitude Southern Hemisphere simulated by a coupled atmosphere-sea ice-ocean-vegetation model, *Holocene*, *15*(7), 951–964, doi:10.1191/0959683605hl869ra.

Risi, C., S. Bony, and F. Vimeux (2008), Influence of convective processes on the isotopic composition ($\delta^{18}O$ and δD) of precipitation and water vapor in the tropics: 2. Physical interpretation of the amount effect, *J. Geophys. Res.*, *113*, D19306, doi:10.1029/2008JD009943.

Risi, C., A. Landais, S. Bony, J. Jouzel, V. Masson-Delmotte, and F. Vimeux (2010a), Understanding the ^{17}O-excess glacial-interglacial variations in Vostok precipitation, *J. Geophys. Res.*, *115*, D10112, doi:10.1029/2008JD011535.

Risi, C., S. Bony, F. Vimeux, and J. Jouzel (2010b), Water-stable isotopes in the LMDZ4 general circulation model: Model evaluation for present-day and past climates and applications to climatic interpretations of tropical isotopic records, *J. Geophys. Res.*, *115*, D12118, doi:10.1029/2009JD013255.

Risi, C., A. Landais, R. Winkler, and F. Vimeux (2013), Can we determine what controls the spatio-temporal distribution of d-excess and ^{17}O-excess in precipitation using the LMDZ general circulation model?, *Clim. Past*, *9*(5), 2173–2193, doi:10.5194/cp-9-2173-2013.

Roche, D. M., X. Crosta, and H. Renssen (2012), Evaluating Southern Ocean sea-ice for the Last Glacial Maximum and pre-industrial climates: PMIP-2 models and data evidence, *Quaternary Sci. Rev.*, *56*, 99–106, doi:10.1016/j.quascirev.2012.09.020.

Roeckner, E., K. Arpe, and L. Bengtsson (1996), The atmospheric general circulation model ECHAM-4: Model description and simulation of present-day climate, *Max-Planck-Institut für Meteorologie Rep.*, *218*, 90.

Scarchilli, C., M. Frezzotti, and P. M. Ruti (2010), Snow precipitation at four ice core sites in East Antarctica: Provenance, seasonality and blocking factors, *Clim. Dyn.*, *37*(9–10), 2107–2125, doi:10.1007/s00382-010-0946-4.

Schmidt, G. A., G. Hoffmann, D. T. Shindell, and Y. Hu (2005), Modeling atmospheric stable water isotopes and the potential for constraining cloud processes and stratosphere-troposphere water exchange, *J. Geophys. Res.*, *110*, D21314, doi:10.1029/2005JD005790.

Schmitt, J., et al. (2012), Carbon isotope constraints on the deglacial CO2 rise from ice cores, *Science*, *336*(6082), 711–714, doi:10.1126/science.1217161.

Schoenemann, S. W., A. J. Schauer, and E. Steig (2013), Measurement of SLAP2 and GISP $\delta^{17}O$ and proposed VSMOW-SLAP normalization for $\delta^{17}O$ and $^{17}O_{excess}$, *Rapid Commun. Mass Spectrom.*, *27*, 582–590, doi:10.1002/rcm.6486.

Sodemann, H., and A. Stohl (2009), Asymmetries in the moisture origin of Antarctic precipitation, *Geophys. Res. Lett.*, *36*, L22803, doi:10.1029/2009GL040242.

Steig, E. J., C. P. Hart, J. W. C. White, W. L. Cunningham, M. D. Davis, and E. S. Saltzman (1998a), Changes in climate, ocean and ice-sheet conditions in the Ross embayment, Antarctica, at 6 ka, *Ann. Glaciol.*, *27*, 305–310.

Steig, E. J., E. J. Brook, J. White, C. M. Sucher, M. L. Bender, S. J. Lehman, D. L. Morse, E. D. Waddington, and G. D. Clow (1998b), Synchronous climate changes in Antarctica and the North Atlantic, *Science*, *282*(5386), 92–95.

Steig, E. J., D. L. Morse, E. D. Waddington, M. Stuiver, P. M. Grootes, P. A. Mayewski, M. S. Twickler, and S. I. Whitlow (2000), Wisconsinan and Holocene climate history from an ice core at Taylor Dome, western Ross Embayment, Antarctica, *Geogr. Ann. A*, *82*(2–3), 213–235.

Stenni, B., J. Jouzel, V. Masson-Delmotte, R. Rothlisberger, E. Castellano, O. Cattani, S. Falourd, S. J. Johnsen, A. Longinelli, and J. P. Sachs (2004), A late-glacial high-resolution site and source temperature record derived from the EPICA Dome C isotope records (East Antarctica), *Earth Planet. Sci. Lett.*, *217*(1-2), 183–195, doi:10.1016/S0012-821X(03)00574-0.

Stenni, B., et al. (2010a), Expression of the bipolar see-saw in Antarctic climate records during the last deglaciation, *Nat. Geosci.*, *4*(1), 46–49, doi:10.1038/ngeo1026.

Stenni, B., V. Masson-Delmotte, E. Selmo, H. Oerter, H. Meyer, R. Rothlisberger, J. Jouzel, O. Cattani, S. Falourd, and H. Fischer (2010b), The deuterium excess records of EPICA Dome C and Dronning Maud Land ice cores (East Antarctica), *Quaternary Sci. Rev.*, *29*(1), 146–159.

Stohl, A., and H. Sodemann (2010), Characteristics of atmospheric transport into the Antarctic troposphere, *J. Geophys. Res.*, *115*, D02305, doi:10.1029/2009JD012536.

Uemura, R., Y. Matsui, N. Yoshida, O. Abe, and S. Mochizuki (2005), Isotopic fractionation of water during snow formation: Experimental evidence of kinetic effect, *Polar Meteorol. Glaciol.*, *19*, 1–14.

Uemura, R., E. Barkan, O. Abe, and B. Luz (2010), Triple isotope composition of oxygen in atmospheric water vapor, *Geophys. Res. Lett.*, *37*, L04402, doi:10.1029/2009GL041960.

Uemura, R., V. Masson-Delmotte, J. Jouzel, A. Landais, H. Motoyama, and B. Stenni (2012), Ranges of moisture-source temperature estimated from Antarctic ice cores stable isotope records over glacial–interglacial cycles, *Clim. Past*, *8*(3), 1109–1125, doi:10.5194/cp-8-1109-2012.

Vimeux, F., V. Masson, G. Delaygue, J. Jouzel, J. R. Petit, and M. Stievenard (2001), A 420,000 year deuterium excess record from East Antarctica: Information on past changes in the origin of precipitation at Vostok, *J. Geophys. Res.*, *106*(D23), 31,863–31,873, doi:10.1029/2001JD900076.

WAIS Divide Project Members (2013), Onset of deglacial warming in West Antarctica driven by local orbital forcing, *Nature*, *1–7*, doi:10.1038/nature12376.

Watanabe, O., J. Jouzel, S. Johnsen, F. Parrenin, H. Shoji, and N. Yoshida (2003), Homogeneous climate variability across East Antarctica over the past three glacial cycles, *Nature*, *422*(6931), 509–512, doi:10.1038/nature01525.

Werner, M., and M. Heimann (2002), Modeling interannual variability of water isotopes in Greenland and Antarctica, *J. Geophys. Res.*, *107*(D1), 4001, doi:10.1029/2001JD900253.

Werner, M., P. M. Langebroek, T. Carlsen, and M. Herold (2011), Stable water isotopes in the ECHAM5 general circulation model: Toward high-resolution isotope modeling on a global scale, *J. Geophys. Res.*, *116*, D15109, doi:10.1029/2011JD015681.

Winkler, R., A. Landais, H. Sodemann, L. Dümbgen, F. Prié, V. Masson-Delmotte, B. Stenni, J. Jouzel, and V. Rath (2012), Deglaciation records of ^{17}O-excess in East Antarctica: Reliable reconstruction of oceanic normalized relative humidity from coastal sites, *Clim. Past*, *8*(1), 1–16.

Winkler, R., A. Landais, C. Risi, and M. Baroni (2013), Interannual variation of water isotopologues at Vostok indicates a contribution from stratospheric water vapor, *Proc. Natl. Acad. Sci. U. S. A.*, *110*, 17,674–17,679.

Wolff, E. W., et al. (2006), Southern Ocean sea-ice extent, productivity and iron flux over the past eight glacial cycles, *Nature*, *440*(7083), 491–496, doi:10.1038/nature04614.

Zahn, A., P. Franz, C. Bechtel, J.-U. Grooß, and T. Röckmann (2006), Modelling the budget of middle atmospheric water vapour isotopes, *Atmos. Chem. Phys.*, *6*(8), 2073–2090.